








Spin state crossover in Co_3BO_5

N. V. Kazak ^{*}, M. S. Platonov, Yu. V. Knyazev , M. S. Molokeyev , M. V. Gorev , and S. G. Ovchinnikov 
Kirensky Institute of Physics, Federal Research Center KSC SB RAS, 660036 Krasnoyarsk, Russia

Z. V. Pchelkina ^{1,2}, V. V. Gapontsev,² and S. V. Streltsov ^{1,2}


¹*M.N. Miheev Institute of Metal Physics UB RAS, 620137 Ekaterinburg, Russia*

²*Ural Federal University, 620002 Ekaterinburg, Russia*

J. Bartolomé ³ and A. Arauzo ^{3,4}

³*Instituto de Nanociencia y Materiales de Aragón (INMA), CSIC-Universidad de Zaragoza and Departamento de Física de la Materia Condensada, 50009 Zaragoza, Spain*

⁴*Servicio de Medidas Físicas, Universidad de Zaragoza, 50009 Zaragoza, Spain*

V. V. Yumashev 

Institute of Chemistry and Chemical Technology, Federal Research Center KSC SB RAS, 660036 Krasnoyarsk, Russia

S. Yu. Gavrilkin

P.N. Lebedev Physical Institute of RAS, 119991 Moscow, Russia

F. Wilhelm and A. Rogalev

ESRF-The European Synchrotron, 71 Avenue des Martyrs CS40220, F-38043 Grenoble Cedex 9, France



(Received 15 September 2020; accepted 8 March 2021; published 31 March 2021)

We have investigated the spin and oxidation states of Co in Co_3BO_5 using x-ray magnetic circular dichroism (XMCD) and dc magnetic susceptibility measurements. At low temperatures, XMCD experiments have been performed at the Co *K*-edge in Co_3BO_5 and Co_2FeBO_5 single crystals in the fully ferrimagnetically ordered phase. The Co (*K*-edge) XMCD signal is found to be related to the Co^{2+} magnetic sublattices in both compounds, providing strong experimental support for the low-spin (LS) Co^{3+} scenario. The paramagnetic susceptibility is highly anisotropic. An estimation of the effective magnetic moment in the temperature range 100–250 K correlates well with two Co^{2+} ions in the high-spin (HS) state and some orbital contribution, while Co^{3+} remains in the LS state. The crystal structure of the Co_3BO_5 single crystal has been solved in detail at the *T* range 296–703 K. The unit cell parameters and volume show anomalies at 500 and 700 K. The octahedral environment of the Co4 site strongly changes with heating. The generalized gradient approximation with Hubbard *U* correction calculations have revealed that, at low-temperatures, the system is insulating with a band gap of 1.4 eV, and the Co^{2+} ions are in the HS state, while Co^{3+} are in the LS state. At high temperatures (*T* > 700 K), the charge ordering disappears, and the system becomes metallic with all Co ions in $3d^7$ electronic configuration and HS state.

DOI: [10.1103/PhysRevB.103.094445](https://doi.org/10.1103/PhysRevB.103.094445)

I. INTRODUCTION

The cobalt oxides belong to a large class of strongly correlated compounds showing the complex interplay between spin, charge, lattice, and orbital degrees of freedom. Like other *3d* transition metals, cobalt exhibits several possible oxidation states— $\text{Co}^{2+}(d^7)$, $\text{Co}^{3+}(d^6)$, and $\text{Co}^{4+}(d^5)$. A property which makes the cobalt oxides very peculiar is the ability of Co^{3+} ions to accommodate various spin states, that is, low spin (LS), high spin (HS), and intermediate spin. The spin state of Co^{3+} appears to be very sensitive to changes in the

Co-O bond length and Co-O-Co bond angle, and a spin state transition could happen under action of temperature, magnetic field, or external pressure. This makes the physics of the cobalt oxides very complicated, being a subject of longstanding controversy [1]. Recently, cobalt-containing oxyborates with a general formula of $M^{2+}_2M'^{3+}\text{BO}_5$ (*M*, *M'* = Co, and *3d* metal ions, as well as Al, Ga, and Mg) have attracted much attention due to the discovery of their intriguing magnetic and electronic behaviors [2–7]. These materials crystallize in orthorhombic structure (space group *Pbam*) and are isostructural to ludwigite mineral. The M^{2+} and M'^{3+} ions are located at the centers of edge-sharing oxygen octahedra, forming linear chains propagating along the short crystallographic direction (*c* ≈ 3 Å). The boron atoms have a trigonal-planar

*nat@iph.krasn.ru

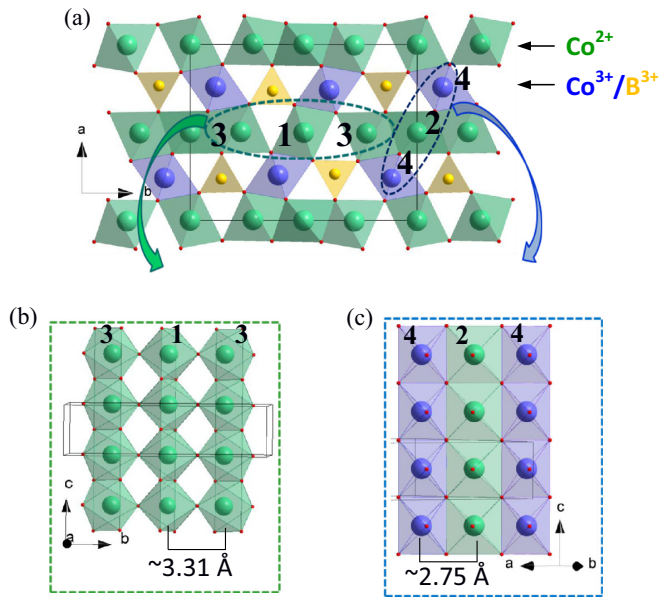


FIG. 1. (a) The ab projection of crystal structure of Co_3BO_5 . The green and blue spheres are octahedrally coordinated divalent and trivalent ions, respectively, that occupy different crystallographic sites 1, 2, 3, and 4. The triangle BO_3 groups are shown in yellow. (b) The triads 3-1-3 with the longest and (c) 4-2-4 with shortest Co-Co distances. Interionic distances are highlighted by dotted lines.

coordination BO_3 , normally linked via common corners with oxygen octahedra. The cations occupy four crystallographically distinct metal sites $2a$, $2b$, $4g$, and $4h$, which are usually numbered as $M1$, $M2$, $M3$, and $M4$, respectively (Fig. 1). The first three are occupied by divalent metal ions, whereas the latter site located in the spaces between BO_3 groups is occupied by the trivalent cations. As a result, a dense crystal structure is formed by alternating layers of divalent and trivalent cations. The triads 3-1-3 and 4-2-4 with longest and shortest interionic distances are structurally, magnetically, and electronically singled out. The common ludwigite structure allows various types of magnetic interactions involving the metal ions, including superexchange interactions, direct exchange interactions, and dipole-dipole interactions, among which the former is dominant.

The homometallic ludwigites Fe_3BO_5 and Co_3BO_5 are the most thoroughly studied systems due to their quite distinct structural, magnetic, and electronic properties [2,4,8]. Fe_3BO_5 demonstrates extremely rich physics and undergoes several transitions upon cooling from room temperature. First, a structural orthorhombic-orthorhombic transition takes place at $T_{st} = 283$ K [$Pbam(N\#55)$ – $Pbnm(N\#62)$], which is accompanied by the formation of the pairs (“dimers”) of Fe^{2+} and Fe^{3+} ions in a 4-2-4 triad [9,10]. The phase transition in Fe_3BO_5 detected by the x-ray diffraction (XRD) also manifests itself in the temperature dependence of electrical resistivity and hyperfine parameters, revealing well-defined anomalies at T_{st} [9,11,12]. With decreasing temperature, a cascade of magnetic transitions is observed by means of magnetometry, Mössbauer, and temperature-dependent neutron diffraction studies [13–15]. At $T_{N1} = 112$ K, the 4-2-4 spin ladder is antiferromagnetically ordered. At $T_{N2} = 74$ K,

the ferrimagnetic ordering in the 3-1-3 spin-ladder appears. Finally, the transition to the antiferromagnetic ground state at $T_{N3} = 30$ K with zero magnetic moment per unit cell is observed. The bulk magnetization measurements revealed that the anisotropy axis changes from the a to the b axis in the low-temperature antiferromagnetic phase.

On the contrary, cobalt ludwigite Co_3BO_5 demonstrates more conventional behavior, with the only ferrimagnetic transition at $T_N = 42$ K and no structural transformations [4,16,17]. The high magnetic uniaxial anisotropy with the b axis as an easy magnetization direction (EMD) was detected in the entire temperature range [15,18]. The remanent magnetization per Co atom is $\sim 1.1 \mu_B$. A small slope of magnetization at high magnetic fields seems to indicate the existence of a more complex magnetic structure.

Over the last decade, attempts to understand the observed difference in magnetic and electronic properties of two homometallic ludwigites led to a synthesis of several new compounds: CoMgGaBO_5 [19], $\text{Co}_{2.4}\text{Ga}_{0.6}\text{BO}_5$ [20], $\text{Co}_{2.88}\text{Cu}_{0.12}\text{BO}_5$ [21], $\text{Co}_{4.76}\text{Al}_{1.24}\text{BO}_5$ [22], Co_2AlBO_5 [23], $\text{Co}_{3-x}\text{Fe}_x\text{BO}_5$ ($0.0 < x < 1.0$) [15,17,18,24,25], $\text{Co}_{1.7}\text{Mn}_{1.3}\text{BO}_5$ [26], $\text{Co}_5\text{TiB}_2\text{O}_{10}$ [27], and $\text{Co}_5\text{SnB}_2\text{O}_{10}$ [28] are some of them. (Here, we do not mention ludwigites based on other $3d$ metals, the studies of which are also numerous.) The main conclusions that can be drawn from these studies are the following: (i) isovalent substitution of Co^{3+} ions by nonmagnetic ions like Ga and Al or magnetic Mn causes an onset of short-range or long-range orderings, but their critical temperatures are found in the vicinity of the T_N characteristic of Co_3BO_5 . The reason, apparently, is the sensitivity of the magnetic subsystem to the cation distribution. (ii) The nonmagnetic substitution of type $2 \cdot \text{Co}^{3+} \rightarrow (\text{Co}^{2+} + M^{4+})$, where $M^{4+} = \text{Ti}$ or Sn , leads to an antiferromagnetic spin ordering at $T_N = 82$ K, i.e., twice of T_N of Co_3BO_5 . Considering that tetravalent substitution generates Co^{2+} ions at the $M4$ site, an increase in the Néel temperature should be attributed to the enhancement of exchange interactions because of the substitution of LS Co^{3+} by the HS Co^{2+} at this site. (iii) An unexpected effect was discovered at the substitution of Co^{3+} by Fe^{3+} ions. In particular, with Fe^{3+} content increase, the samples exhibit a magnetic transition at 83 K, which is then split into two magnetic transitions at 77 and 86 K [25], and finally, the Fe^{3+} -rich sample Co_2FeBO_5 shows antiferromagnetic ($T_{N1} = 110$ K) and ferrimagnetic-like ($T_{N2} = 70$ K) transitions like the end compound Fe_3BO_5 [15,18]. An analysis of the Co-containing ludwigite systems indicates that the chemical substitution modifies the magnetically active subsystem only if it results in the appearance of magnetic ions at the $M4$ site (Co^{2+} , Mn^{3+} , or Fe^{3+}).

Based on the low-temperature neutron diffraction, Freitas *et al.* [29] have found a rather small magnetic moment ($\sim 0.5 \mu_B$) for Co ions occupying the $M4$ site, instead of the expected $4 \mu_B$ for HS Co^{3+} ($t_{2g}^4 e_g^2$, $S = 2$), while the observed moments of Co at the $M1$ site ($\sim 3.6 \mu_B$), at the $M2$ site ($3.1 \mu_B$), and at the $M3$ site ($3.8 \mu_B$) are consistent with those expected for HS Co^{2+} ions ($t_{2g}^5 e_g^2$, $S = \frac{3}{2}$). It was then assumed that Co^{3+} ions in Co_3BO_5 are in the LS state ($t_{2g}^6 e_g^0$, $S = 0$). It was found also that all magnetic moments are almost parallel to the b axis, making it an EMD. The spin

ordering within the 3-1-3 triad is antiferromagnetic ($\uparrow\downarrow\uparrow$). These triads are ferromagnetically coupled with each other via Co ions at the $M2$ site, resulting in the total uncompensated magnetic moment $\sim 1.4 \mu_B$ per Co ion. The recent measurements of crystal structure, magnetic susceptibility, electrical conductivity, and soft x-ray spectroscopy of Co_3BO_5 performed in the paramagnetic regime $T = 300\text{--}700$ K revealed the existence of two phase transitions at 475 and 495 K [30]. These transitions are well-defined from the differential scanning calorimetry (DSC) and electrical conductivity experiments and are accompanied by anomalies in the unit cell parameters, although the type of crystal structure is retained, and the space group remains unchanged ($Pbam$). A large paramagnetic moment $4.87 \mu_B$ per Co ion was obtained from the fit of high-temperature part of magnetic susceptibility above room temperature, and a deviation from Curie-Weiss behavior below this temperature was found. Although direct experimental evidence of spin transition is still missing, the authors [30] deduced that Co_3BO_5 undergoes a gradual Co^{3+} spin-state crossover in the temperature interval $T_N \leq T < 300$ K and two-step changes in the Co oxidation state in each of four crystallographic sites at high temperatures. Indeed, the effective magnetic moment $\mu_{\text{eff}} = 4.16 \mu_B/\text{Co}$ obtained from the fitting of the susceptibility in the interval $T = 100 - 300$ K [16,18] can be compared with the value $\mu_{\text{eff}} = 4.24 \mu_B$ expected for the case in which all Co ions, including the trivalent ones, are in HS states (without orbital moment contribution). This observation indicates that a crossover or a transition from LS to HS could occur in Co_3BO_5 . However, the study of thermodynamic properties of Co_3BO_5 below room temperature [16] did not reveal any anomaly except the magnetic one at $T_N = 42$ K. At the same time, conductivity and DSC measurements [30] performed on both single crystalline and powder samples at $T > 300$ K showed anomalies, which are typically associated with a first-order phase transition. Consequently, the magnetic properties and origin of the magnetic moments in the Co_3BO_5 remain unclear.

Thus, the subject of this paper is to determine the spin and oxidation states of cobalt ions in Co_3BO_5 and to study their evolution with temperature. We have performed single-crystalline XRD, DSC, and heat capacity measurements in a wide temperature range of 296–773 K. The Co K -edge x-ray magnetic circular dichroism (XMCD) and angle-dependent dc susceptibility experiments were carried out in the ferrimagnetic phase (~ 5 K) and above the magnetic phase transition (100–250 K), respectively. We calculated the electronic structure and magnetic moments of Co atoms at different metal sites for two paramagnetic phases: 296 K (low-temperature phase) 703 K (high-temperature phase) using the density functional theory (DFT) with the account of strong Coulomb correlations through the generalized gradient approximation with Hubbard U correction (GGA + U) scheme.

These combined experimental and theoretical studies indicate that, at temperatures up to room temperature, the magnetic lattice of Co_3BO_5 is formed mostly by divalent Co^{2+} ions ($S = \frac{3}{2}$ with a small orbital contribution), while Co^{3+} is in the LS state. The high-temperature investigation of crystal structure did not reveal any structural transformations (space group $Pbam$), whereas the lattice parameters and volume show a large thermal expansion and anomalies at

$T_1 = 500$ and $T_2 = 700$ K. The unit cell volume increases by about 4.5%. We found that the octahedral environment of Co ions at the $M4$ site is drastically changed. The measurements of DSC indicate that the compound does not experience any first- or second-order phase transitions besides those into the magnetically ordered state at T_N . This is confirmed by the thermodynamic property measurements, which revealed the existence of two smeared anomalies in the high-temperature range which are consistent with those observed in the XRD experiments.

Our GGA + U calculations have shown, first of all, that the Co^{2+} ions are in the HS state, while Co^{3+} are in the LS state at low temperatures. Second, in the high-temperature phase ($T = 703$ K), the charge ordering disappears, all Co ions have the same $3d^7$ electronic configuration, and the system becomes metallic with all Co ions in the HS state. Moreover, our calculations point out that the spin-state transition and charge ordering does not necessarily occur at the same temperature.

II. EXPERIMENTAL TECHNIQUES AND DETAILS OF THE CALCULATION

Needle-shaped single crystalline specimens of Co_3BO_5 were synthesized using a flux method in the system $\text{Bi}_2\text{Mo}_3\text{O}_{12}\text{-B}_2\text{O}_3\text{-CoO-Na}_2\text{CO}_3\text{-Co}_2\text{O}_3$ [18].

X-ray absorption near-edge structure (XANES) and x-ray magnetic circular dichroism (XMCD) measurements at the K -edges of Co and Fe were performed at the ESRF ID12 beamline. The first harmonic of APPLE-II type helical undulator was used as a source of circularly polarized x rays. To further monochromatize the undulator emission, a fixed-exit double crystal Si(111) monochromator was used at the required photon energies. The single crystals of Co_3BO_5 and Co_2FeBO_5 were mounted on a cold finger of an “amagnetic” He flow cryostat that was inserted in a cold bore of superconducting solenoid producing a maximum magnetic field of 17 Tesla. All XANES spectra were recorded using total fluorescence yield detection mode in “back-scattering” geometry using Si photodiodes mounted on the liquid nitrogen shield of the solenoid, allowing very large solid angle of detection. Experiments were performed at 5 K under a magnetic field of ± 17 T to ensure that the magnetic saturation was reached. Samples were oriented so that the direction of the magnetic field and incident x-ray wavevector were collinear with the crystallographic b axis, which is an EMD for both samples. The normalized XANES spectra were corrected for self-absorption effects, considering the various background contributions (fluorescence of outer electronic subshells and other elements in the sample as well as coherent and incoherent scattering) and the solid angle of the detector. The XMCD signal was obtained as the direct difference of XANES spectra measured with opposite helicities of the light at a fixed magnetic field. The resulting XMCD spectra are measured repeatedly with the opposite direction of magnetization to eliminate any artifacts.

For magnetic measurements, a single crystal of 0.41 mg was mounted in the rotator option of a superconducting quantum interference device-based magnetometer. The sample was fixed with a pinch of vacuum grease with the rotator axis parallel and perpendicular to the needle axis (c axis). We could

select the different a , b , and c axis for the measurements as a function of temperature. dc magnetic susceptibility at 1 kOe has been measured from 100 to 250 K at different orientations.

The simultaneous thermal analysis (STA) of the Co_3BO_5 sample was performed using the Jupiter STA 449C analyzer (NETZSCH, Germany) equipped with an Aëolos QMS 403C quadrupole mass spectrometer (NETZSCH, Germany) in Pt-Rh crucibles. A powdered sample of Co_3BO_5 single crystals with a weight of 160 mg was used. The conditions of the experiment in Ref. [30] were reproduced except for the temperature range, which was slightly shifted to the high-temperature range of 373–773 K due to instrumental limitations, while being in the range of the thermal effects observed by the authors in Ref. [30]. The measurements of mass change (TG) and heat flux (DSC) was performed in sequential heating and cooling mode at a rate of 10 °C/min within temperature range 373–73 K, supplying the different gas mixtures (20 vol.% O_2 in Ar and Ar with purity 99.9995 vol.%) with total flow rate of 50 cm³(NTP)/min. Two successive heating-cooling cycles were carried out for each gas mixture. The first heating-cooling cycle was used for sample conditioning and the second cycle for data processing.

The specific heat capacity data from 373–773 K were obtained by the “ratio method” using a differential scanning calorimeter Netzsch STA Jupiter 449 C equipped with a special sample holder for C_p measurements. Three different runs under the same conditions (dynamic argon-oxygen atmosphere 20 vol.% O_2 , the heating rate 10 K/min) were carried out: (1) the baseline (empty Pt-Rh crucibles with perforated lids); (2) a standard sapphire disk (112 mg, with diameter of 6 mm and height of 1 mm) in the sample crucible; and (3) the powder sample of Co_3BO_5 (60 mg) was manually sealed in the sample crucible. For enhancement of precise determination of heat capacity, it is advantageous when the “thermal masses” of the sapphire and the sample are approximately equivalent, i.e., $(m_{\text{st}} \times C_{p,\text{st}}) \approx (m_{\text{sa}} \times C_p)$.

The specific heat capacity of the sample was determined on the corrected DSC curves according to equation

$$C_p = \frac{m_{\text{st}} (DSC_{\text{sa}} - DSC_{\text{bl}})}{m_{\text{sa}} (DSC_{\text{st}} - DSC_{\text{bl}})} C_{p,\text{st}},$$

where $C_{p,\text{st}}$ is the tabulated specific heat of the standard at temperature T ; m_{st} , m_{sa} are masses of the standard and the sample; DSC_{sa} , DSC_{st} , and DSC_{bl} are the value of DSC signal at temperature T from the sample, the standard, and the baseline curve, respectively. The relative error of C_p measurements did not exceed $\pm 1\%$.

The low-temperature part of specific heat was measured by a relaxation technique in the temperature range 2–300 K on a single crystalline sample with a mass of 3.5 mg using a commercial instrument (Quantum Design PPMS).

The XRD patterns were collected from a single crystal of Co_3BO_5 at 296, 403, 503, 603, and 703 K using the SMART APEX II single crystal diffractometer (Bruker AXS, analytical equipment) equipped with a PHOTON 2 CCD-detector, graphite monochromator and Mo $K\alpha$ radiation source. The measurements were carried out in the Common Access Facility Centre of SB RAS in Krasnoyarsk. The space group was defined by the analysis of extinction rules and intensity statistics obtained from all reflections. Multiscan absorption

correction of reflection intensities was performed with the SADABS program. Then the intensities of equivalent reflections were averaged. We note that face-indexed absorption correction could not be applied because one of the crystal faces was irregular, and the thermal paste used to fix and protect the sample in the high-temperature experiments prevented us from applying the edge method. The structure was solved by direct methods [31] using the SHELXS program. The structure refinement was carried out by least-square minimization in the SHELXL program [32] using anisotropic thermal parameters of all atoms.

The electronic structure of Co_3BO_5 was calculated within the DFT using the Vienna *Ab initio* Simulation Package (VASP) [33]. The Perdew-Burke-Ernzerhof (PBE) version of the exchange-correlation potential [34] was utilized. For the Brillouin zone integration, a $8 \times 8 \times 16$ Monkhorst-Pack mesh was used. The cutoff energy for the plane-wave basis was set to 500 eV. The total energy calculations were performed within GGA + U in rotationally invariant form [35]. The values of onsite Coulomb repulsion and Hund’s exchange were taken to be $U = 7$ eV and $J_H = 0.9$ eV, respectively [36].

III. RESULTS AND DISCUSSION

A. XMCD magnetometry

The element-selective XMCD spectroscopy allows us to determine the magnetic behavior of the different elements in complex materials through the disentanglement of their contributions to the total magnetic response or to compare the magnetic behavior of a chosen element in different materials. Here, we focus on the isostructural compounds Co_3BO_5 and Co_2FeBO_5 .

In Co_2FeBO_5 , the Fe^{3+} ions substitute Co^{3+} ions at $M4$ sites as it was found from XRD and Mössbauer spectroscopy studies [18,37]. This material has a high magnetic uniaxial anisotropy with the b axis as an EMD inherent to Co_3BO_5 and undergoes ferrimagnetic ($T_{N_2} = 70$ K) and antiferromagnetic ($T_{N_1} = 115$ K) transitions like Fe_3BO_5 revealing a great impact of the magnetic ion at the $M4$ site. The Co_2FeBO_5 displays a strong reduction of the remanent magnetization compared with Co_3BO_5 . Assuming the LS state of Co^{3+} , one might expect a large uncompensated magnetic moment in the 4-2-4 triad, and hence, in all the unit cell (this is a crude approximation since there is never the situation where all Co^{3+} ions are in LS), while the appearance of the ion with a nonzero magnetic moment at the $M4$ site should result in the decrease of the moment under the condition of the antiparallel arrangement of this moment relative the host magnetic system of Co^{2+} . Indeed, the remanent magnetization in Co_3BO_5 was found to equal $M_r \approx 72$ emu/g, whereas in Co_2FeBO_5 , the M_r is reduced to 20 emu/g [18]. Based on the neutron powder diffraction and the angle-dependent magnetization data, the schematic representation of magnetic couplings in Co_3BO_5 and Co_2FeBO_5 can be presented as shown in Fig. 2.

The Co^{3+} ion in LS state does not have unpaired spins ($t_{2g}^6 e_g^0, S = 0$), and therefore, it should not contribute to the magnetic moment of Co_3BO_5 . If this is the case, the Co^{2+} ions, residing at the 3-1-3 triads and site 2 of the 4-2-4

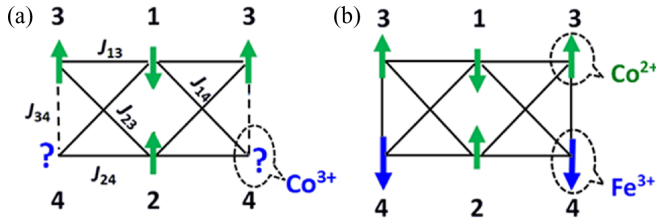


FIG. 2. Schematic representation of magnetic couplings in (a) Co_3BO_5 and (b) Co_2FeBO_5 . The direction of Co^{2+} and Fe^{3+} magnetic moments shown by the green and blue arrows, respectively, reflects the antiferromagnetic coupling between two subsystems. The question mark underlines the hypothesis of $M4$ site being occupied mainly by Co^{3+} ions. The magnetic moments of Co^{3+} ions are not shown. The solid lines denote the superexchange interactions between the nearest magnetic ions $\text{Co}^{2+}\text{-O-Co}^{2+}$ and $\text{Co}^{2+}\text{-O-Fe}^{3+}$ (J_{ij}), while the dashed line is the magnetic coupling $\text{Co}^{2+}\text{-O-Co}^{3+}$. More detailed consideration on superexchange interactions in the ludwigites is presented in Ref. [38].

triads, should resemble those in $\text{Co}_2^{2+}\text{Fe}^{3+}\text{BO}_5$ (this is a crude approximation since the Fe^{3+} ion is magnetic and is certainly coupled to the Co^{2+} sublattice in the 4-2-4 triads).

To directly address the problem of the spin state of Co^{3+} ions, the XMCD experiment was performed at the Co K -edge under the same temperature and field conditions on both Co_3BO_5 and Co_2FeBO_5 single crystals. The fully ferrimagnetically ordered phases were considered. The XMCD spectra are shown in Fig. 3(b) along with corresponding normalized XANES spectra [Fig. 3(a)]. The pre-edge peak, which is sensitive to the orbital component of the magnetic moment, was analyzed. This hard x-ray spectroscopy probes the transitions from a $1s$ core state to the empty $4p$ states, and the pre-edge feature (7710–7715 eV) arises from transitions to more localized unoccupied $3d$ states, resulting from the $\text{Co}4p\text{-}3d$ hybridization. While the shapes of $\text{Co}(K)$ XANES spectra are very similar for both samples, a significant difference in their intensity is seen. This is related to the changes of local symmetry around Co atoms. Because the cobalt local symmetry and magnetization probed by XANES/XMCD provide information averaged over all nonequivalent crystallographic positions of Co, the shape and the intensity of the spectra measured at Co K -edge is expected to be dependent on the samples. The intensity of the XANES pre-edge feature is reduced in the Co_2FeBO_5 sample relative to that of Co_3BO_5 indicating both the $4p\text{-}3d$ hybridization and the number of the unoccupied $3d$ states are different. A clear XMCD signal is visible at the pre-edge feature of Co. A nonzero XMCD signal reflects the magnetic polarization of the Co $4p$ band resulting from the intra-atomic exchange interaction with the $3d$ band.

The sign of the Co K -edge XMCD signal implies that, in both Co_3BO_5 and Co_2FeBO_5 , the magnetization of the Co sublattice is parallel to the applied magnetic field. The shape of the Co K -edge XMCD spectra is very similar for Co_3BO_5 and Co_2FeBO_5 , while the signal amplitude at the pre-edge feature enhances as the Co^{3+} ions are replaced by Fe^{3+} ions. Then we can assume that the Co K -edge XMCD prepeak (7710–7715 eV) spectrum of Co_3BO_5 is composed of the Co^{2+} component, $\text{XMCD}_{\text{Co}^{2+}}$, and a contribution from Co^{3+} ,

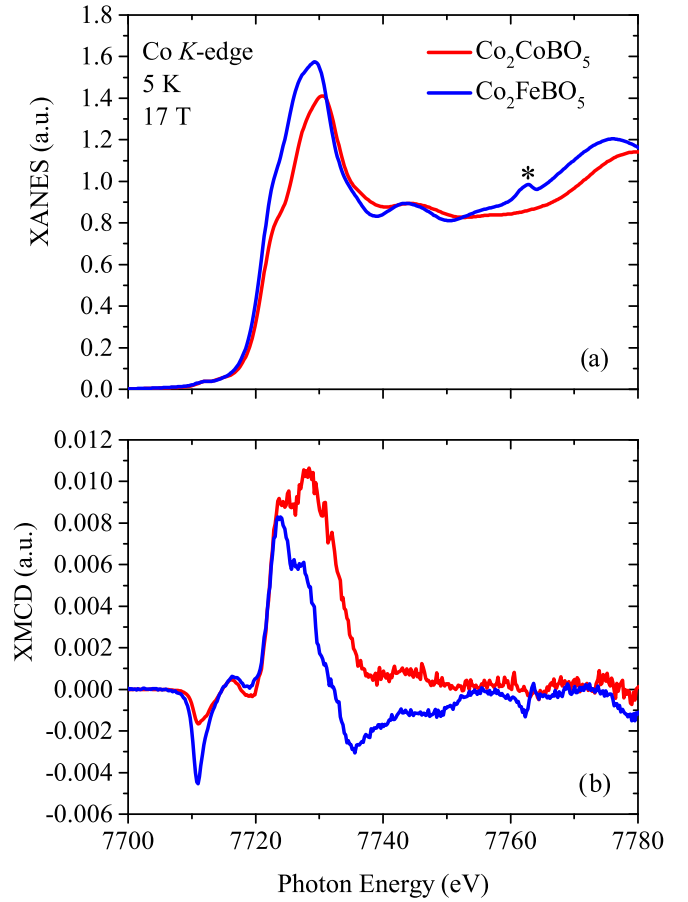


FIG. 3. Normalized Co K -edge (a) x-ray absorption near-edge structure (XANES) and (b) x-ray magnetic circular dichroism (XMCD) spectra recorded at $T = 5$ K and applied field 17 T for Co_3BO_5 and Co_2FeBO_5 single crystals. The asterisk denotes the diffraction peak from the crystal.

$\text{XMCD}_{\text{Co}^{3+}}$, while the XMCD signal of Co_2FeBO_5 depends on the $\text{XMCD}_{\text{Co}^{2+}}$ component only:

$$\text{XMCD}(\text{Co}_2\text{Co}) = \frac{1}{3}(2\text{XMCD}_{\text{Co}^{2+}} + \text{XMCD}_{\text{Co}^{3+}}),$$

$$\text{XMCD}(\text{Co}_2\text{Fe}) = \frac{1}{2}(2\text{XMCD}_{\text{Co}^{2+}}).$$

The signal ratio is determined as follows

$$\frac{\text{XMCD}(\text{Co}_2\text{Co})}{\text{XMCD}(\text{Co}_2\text{Fe})} = \frac{2}{3} \left(1 + \frac{\text{XMCD}_{\text{Co}^{3+}}}{2\text{XMCD}_{\text{Co}^{2+}}} \right).$$

If the Co^{3+} ions in Co_3BO_5 are in the LS state, they should not play any significant role in the magnetic polarization of the Co(sp) band and, consequently, in the Co K -edge XMCD spectra. If this is the case, the signal ratio should be close to 0.66. Any magnetic contribution of the Co^{3+} ions increases this ratio. The magnitude of the XMCD signal was determined by the integration of the XMCD spectrum in the range of the quadrupole transition, and the energy interval was 7705–7715 eV. The ratio of the signals obtained in this way gives the value of 0.70 ± 0.01 . This result shows that there is a rather small net Co^{3+} magnetization in Co_3BO_5 , and this provides experimental support for the LS state of the Co^{3+} ions. The small

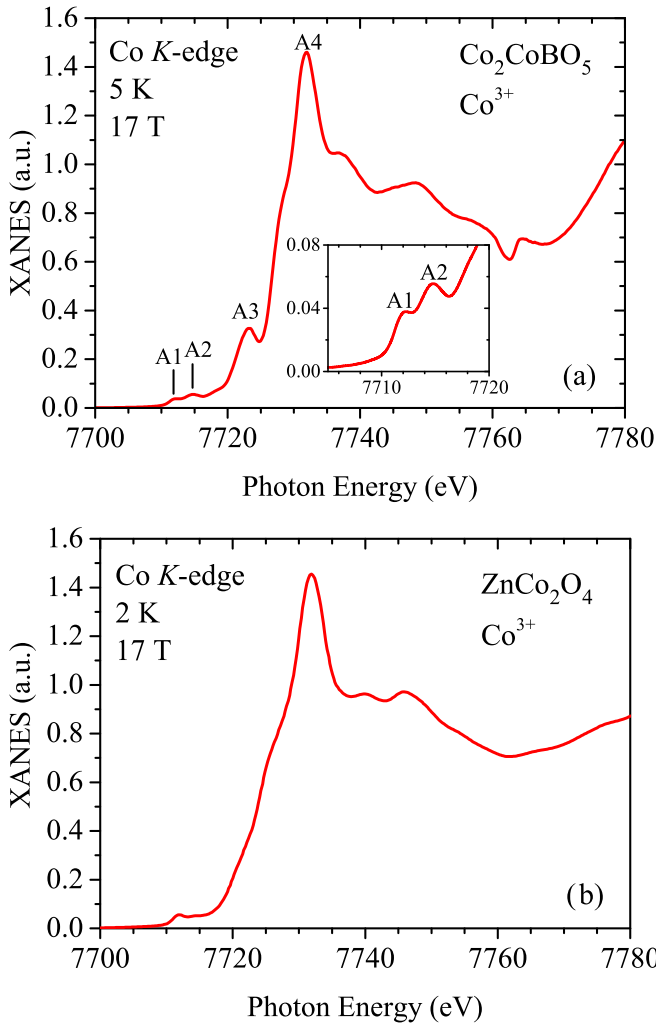


FIG. 4. (a) X-ray absorption near-edge structure (XANES) spectrum corresponding to the Co^{3+} ion in Co_3BO_5 obtained by subtracting of 2XANES spectrum of Co_2FeBO_5 from 3XANES spectrum of Co_3BO_5 . (b) XANES spectrum recorded at the Co K -edge for the spinel ZnCo_2O_4 , data are taken from the Ref. [42].

difference in signals can be explained also by the difference in the contributions of the Co^{2+} sublattice in the direction of applied magnetic field in the two studied compounds.

In the framework of the additivity model, the Co K -edge XANES spectrum of Co_2CoBO_5 is composed of a Co^{2+} component, $\text{XANES}_{\text{Co}^{2+}}$, and a Co^{3+} one, $\text{XANES}_{\text{Co}^{3+}}$. We can assume that the contribution of the Co^{2+} to the Co K -edge XANES spectra is the same for Co_2CoBO_5 and Co_2FeBO_5 compounds, and by subtracting the $\text{XANES}_{\text{Co}^{2+}}$ spectrum, the contribution of the Co^{3+} to the XANES spectrum of Co_2CoBO_5 can be extracted. The $\text{XANES}_{\text{Co}^{3+}}$ spectrum obtained in this way corresponds to the Fe^{3+} atom substituted for Co^{3+} [Fig. 4(a)]. The following noticeable features can be distinguished in the $\text{XANES}_{\text{Co}^{3+}}$ spectrum. The first one is the pre-edge feature which is well resolved [the inset to Fig. 4(a)] and composed of two peaks at 7712.2 eV (A1) and 7714.8 eV (A2). Such a doublet structure was observed earlier in a wide range of x-ray absorption spectroscopy experimental results obtained on the perovskitelike cobaltites LaCoO_3

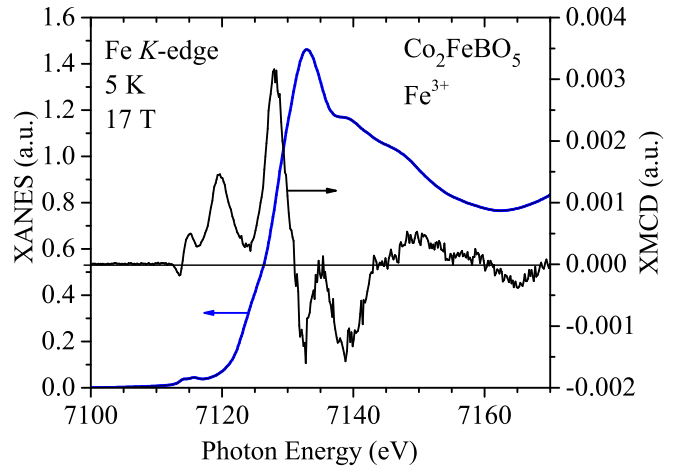


FIG. 5. Normalized Fe K -edge x-ray absorption near-edge structure (XANES)/x-ray magnetic circular dichroism (XMCD) spectra for Co_2FeBO_5 single crystals, $T = 5$ K, and applied field is 17 T.

and GdCoO_3 [39,40]. This pre-edge feature can be assigned to the $1s - 3d$ transition, which is forbidden in the dipole approximation, but it manifests itself due to the $p-d$ orbital mixing and quadrupole contribution. The energy separation of about 2.6 eV is close to the 2.3 and 2.6 eV found in LaCoO_3 [39,40] and GdCoO_3 [41], respectively. A rather intense feature arises at ~ 7723 eV (A3), followed by a sharp increase in the absorption with an energy position of 7732 eV (A4). The latter corresponds to the main $1s-4p$ transition for the Co^{3+} ions, while the former is caused by the same transition in the Co^{2+} ions. Thus, the A3 peak reflects the small difference in the number of Co^{2+} ions per formula unit (f.u.) between both compounds Co_3BO_5 and Co_2FeBO_5 . It is interesting to compare the spectrum of $\text{XANES}_{\text{Co}^{3+}}$ in Co_3BO_5 with the XANES at the Co K -edge for spinel ZnCo_2O_4 measured at the same temperature and field conditions [Fig. 4(b)] [42]. The latter compound is a known p -type conducting oxide material in which Co^{3+} is incorporated at octahedral sites (Co_{Oh}). The Co(K -edge) XANES spectra of both materials are virtually identical, showing the onset of the Co main absorption at the same energy (7732 eV). This observation clearly reveals the presence of trivalent cobalt in Co_3BO_5 ludwigite at low temperatures. Moreover, the shift of the main absorption to higher energies compared with that in Co_2FeBO_5 (7729 eV) reflects the difference in Co^{3+} and Co^{2+} valence states and is comparable with so-called chemical shift usually observed in Co-oxides [42].

The Fe K -edge XANES/XMCD spectra recorded on Co_2FeBO_5 are shown in Fig. 5. The XANES spectrum exhibits two main features: the pre-edge peak located at ~ 7115 eV, which is attributed to the Fe^{3+} ions occupying the octahedrally coordinated sites, and the main edge at ~ 7130 eV, which dominates the XMCD signal. The shape of the XMCD spectrum is different from that observed in $\text{Ho}_{0.5}\text{Nd}_{0.5}\text{Fe}_3(\text{BO}_3)_4$ borate [43] and shows a four-peak structure: one negative and three positive ones. The peak intensity (7120 eV) reaches 0.25%. This value is about one order of magnitude larger than that measured in rare-earth

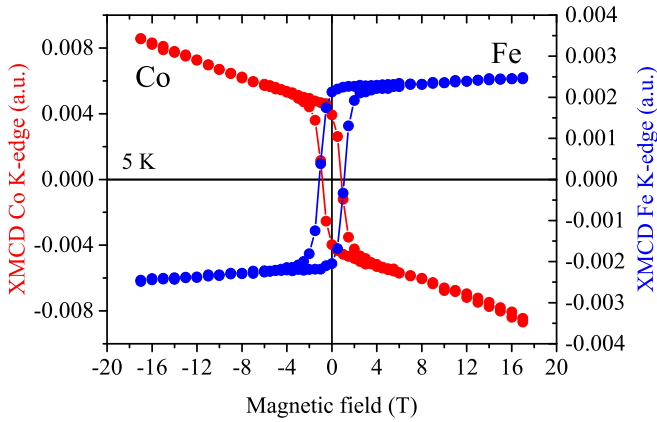


FIG. 6. The element-selective magnetization curves of Co_2FeBO_5 single crystal recorded at Co and Fe K -edges for applied field along the easy magnetization direction (EMD; b axis) and $T = 5$ K.

ferroborate and is comparable with the amplitude obtained for pure Fe foil [44], showing that Fe sublattice is nearly magnetically saturated in Co_2FeBO_5 .

Another interesting feature from the XMCD study is that it provides a simple explanation to the reduction of the magnetic moment under the substitution of Co^{3+} for Fe^{3+} . The element-selective magnetization curves recorded at Co and Fe K -edges present hysteresis loops with opposite signs (Fig. 6). This observation clearly indicates an antiferromagnetic coupling between Co and Fe subsystems and is in line with our previous XMCD measurements at the $L_{2,3}$ edges [45]. The Fe magnetization curve almost reaches saturation, while the Co magnetization curve has a slope highlighting the ferrimagnetic arrangement of cobalt magnetic moments in the Co_2FeBO_5 . Besides the external magnetic field H , which determines the alignment for all magnetic moments and defines the positive direction, two exchange fields act on the Fe magnetic moments: the exchange field $H_{\text{ex}}^{\text{Fe-Fe}}$ created by Fe spins, which favors the parallel alignment of all Fe moments, and the $H_{\text{ex}}^{\text{Fe-Co}}$ created by the Co moments. Similar contributions are acting on the Co magnetic moments: H , $H_{\text{ex}}^{\text{Co-Co}}$, $H_{\text{ex}}^{\text{Co-Fe}}$. The fact that the Co magnetization has the same orientation in both Co_3BO_5 and Co_2FeBO_5 , i.e., positive with respect to the applied field H , indicates that the Co magnetic subsystem determines the trend in the magnetization of the ludwigites. In the ferrimagnetic phase, where exchange fields are larger than H , the $H_{\text{ex}}^{\text{Fe-Co}}$ tends to align the Fe moments antiparallel to the Co ones and, consequently, to H . This magnetic coupling seems to be the strongest if we assume that ordering temperature (T_{N1}) reflects the scale of exchange interactions. As a result, the bulk magnetization of the Fe-substituted ludwigite is significantly reduced due to partial compensation of Co and Fe magnetic moments.

The enhanced impact of Co contribution to the overall magnetization can be explained by the presence of a noticeable orbital moment m_L of the Co^{2+} ion, which is only partially quenched. At low T , the orientation of m_L is determined by both H and the intra-atomic spin-orbit coupling H_{LS} , which according to Hund's third rule favors the parallel

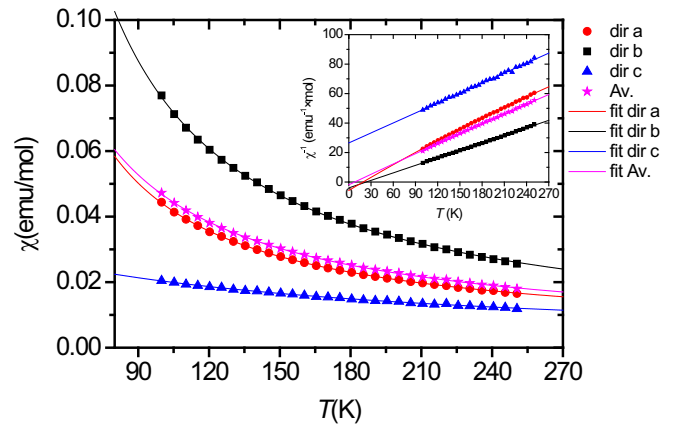


FIG. 7. Temperature dependence of magnetic susceptibility for Co_3BO_5 single crystal in applied field oriented parallel to the a , b , and c axes. Symbols denote the experimental data, the straight lines are fitting using Eq. (1). The averaged susceptibility $\chi_{\text{av}} = \frac{1}{3}(\chi_a + \chi_b + \chi_c)$, denoted by 'Av.', and the corresponding fit to Eq. (1) is also included. Inset: χ^{-1} vs T curves and Curie-Weiss fits.

alignment of the orbital (m_L) and spin (m_S) moments of the Co^{2+} ion.

The experimental changes in the Co K -edge XMCD for two Co-containing ludwigites, supplemented by measurements at the Fe K -edge, were found to correlate with the overall magnetism of the system $\text{Co}_{3-x}\text{Fe}_x\text{BO}_5$ ($x = 0.0$ and 1.0) and qualitatively agree quite well with the magnetic order proposed in Fig. 2. Our results underline the key role of the $M4$ ion because it is the filling of this site by different magnetic ions which leads to the dramatic modification of the magnetic ground state. The $\text{XANES}_{\text{Co}^{3+}}$ spectrum reveals features and onset of Co main absorption like those observed in spinel ZnCo_2O_4 , providing evidence of trivalent cobalt in Co_3BO_5 . We find that it is better to view these ludwigites in terms of Co^{2+} and $M^{3+} = \text{Co}, \text{Fe}$ sublattices. In summary, the XMCD measurements have shown that the magnetism of the Co^{2+} sublattice has a similarity in two isostructural compounds Co_3BO_5 and Co_2FeBO_5 , and the contribution from the Co^{3+} ion is strongly suppressed in Co_3BO_5 .

B. Paramagnetic contribution of Co_3BO_5 as a function of crystal orientation

To study the Co^{3+} contribution in magnetism of Co_3BO_5 in the paramagnetic state, we have performed orientation-dependent susceptibility measurements on a Co_3BO_5 needle-shaped single crystal at temperature range 100–250 K.

Results of the magnetic characterization measurements are presented in Fig. 7. The paramagnetic susceptibility of Co_3BO_5 is highly anisotropic, where the b axis is an EMD, and the c axis is a hard magnetization one. The measurements in green were done with the sample oriented with the c axis perpendicular to the field direction and directly placed on a measuring straw, i.e., without the rotator sample holder. This method circumvents the setback of subtracting the rotator plate contribution to the susceptibility. The χT is relatively flat for this measurement. The measurements with the rotator

TABLE I. Magnetic parameters of Co_3BO_5 extracted in the paramagnetic phase.

	χ_0 (emu/mol)	C (emu · K/mol)	θ (K)	μ_{eff} (μ_B /f.u.)	
<i>a</i> axis	$2.2 \pm 0.2 \times 10^{-3}$	3.3 ± 0.1	21 ± 1	5.1 ± 0.1	IMD
<i>b</i> axis	$0.0 \pm 0.5 \times 10^{-3}$	5.9 ± 0.1	22 ± 1	7.0 ± 0.1	EMD
<i>c</i> axis	$0.0 \pm 0.1 \times 10^{-2}$	4.4 ± 0.6	-118 ± 20	5.9 ± 0.4	HMD
Average	$1.3 \pm 0.3 \times 10^{-3}$	4.0 ± 0.1	11 ± 2	5.7 ± 0.1	

Abbreviations: IMD = intermediate magnetization direction; HMD = hard magnetization direction.

have some drift which can be due to the inherent error in the background measurement which presents some orientation dependence (7–10% deviations). Therefore, these curves were fitted considering a temperature-independent contribution (inset to Fig. 7).

The temperature dependence of the magnetic susceptibility in the paramagnetic state obeys the Curie-Weiss law,

$$\chi = \chi_0 + \frac{C}{T - \theta}. \quad (1)$$

Fitting the data yields a temperature independent term χ_0 , the Curie-Weiss constant C , and the Curie-Weiss temperature θ collected in Table I.

The Curie-Weiss constant C reflects strong anisotropy in the paramagnetic state. The fit to the averaged susceptibility $\chi_{\text{av}} = \frac{1}{3}(\chi_a + \chi_b + \chi_c)$ yields $C = 4.0 \pm 0.1$ (emu · K/mol), resulting in an effective magnetic moment $\mu_{\text{eff}} = 5.7 \pm 0.1 \mu_B$ /f.u., which corresponds to a moment of $3.3 \pm 0.1 \mu_B$ per Co ion. This value is much lower than the previously reported ones [16, 18].

To compare this experimental value of μ_{eff}^S with the possible spin configurations, one has to consider that the average magnetic moment of Co in Co_3BO_5 depends on the number of magnetically active ions $n_{\text{Co}^{2+}}$, $n_{\text{Co}^{3+}}$, on the g factors $g_{\text{Co}^{2+}}$ and $g_{\text{Co}^{3+}}$ and on the spin values $S_{\text{Co}^{2+}}$ and $S_{\text{Co}^{3+}}$ of Co^{2+} and Co^{3+} ions, respectively:

$$\mu_{\text{eff}}^S = \sqrt{\frac{n_{\text{Co}^{2+}} g_{\text{Co}^{2+}}^2 S_{\text{Co}^{2+}} (S_{\text{Co}^{2+}} + 1) + n_{\text{Co}^{3+}} g_{\text{Co}^{3+}}^2 S_{\text{Co}^{3+}} (S_{\text{Co}^{3+}} + 1)}{n_{\text{Co}^{2+}} + n_{\text{Co}^{3+}}}}. \quad (2)$$

(i) Assuming that all magnetic ions are in HS state, the spin-only magnetic moment comprises magnetic moments of Co^{2+} ($n_{\text{Co}^{2+}} = 2$) and Co^{3+} ($n_{\text{Co}^{3+}} = 1$) ions with spin values of $S_{\text{Co}^{2+}}^{\text{HS}} = \frac{3}{2}$ and $S_{\text{Co}^{3+}}^{\text{HS}} = 2$, and $g_{\text{Co}^{3+}} = g_{\text{Co}^{2+}} = 2$. This gives an effective spin moment of $\mu_{\text{eff}}^S = 4.24 \mu_B/\text{Co}$ (right panel of Fig. 8).

(ii) If the Co^{3+} ions are in the LS state ($S_{\text{Co}^{3+}}^{\text{LS}} = 0$) and the Co^{2+} ions are still in HS state, the magnetic moment is reduced to $\mu_{\text{eff}}^S = 3.16 \mu_B/\text{Co}$, which is rather close to the experimental value ($3.3 \mu_B/\text{Co}$), represented by a cross (p.w. = present work) at the right side of Fig. 8, for $n_{\text{Co}}/\text{f.u.} = 3$.

(iii) If only two Co^{2+} ions are contributing in magnetism of Co_3BO_5 , i.e., $n_{\text{Co}^{2+}} = 2$ and $n_{\text{Co}^{3+}} = 0$, the experimentally observed effective spin moment per Co^{2+} ion would be $4.0 \mu_B$, very close to obtained values in the literature for Co^{2+} in octahedral sites ($4.7 - 5.2 \mu_B$), where an orbital contribution is rather important [46]. This case is represented by a cross at the left side of Fig. 8, for $n_{\text{Co}}/\text{f.u.} = 2$.

Usually, for divalent cobalt ions, the observed values of the $g_{\text{Co}^{2+}}$ are significantly > 2 due to the orbital contribution. The experimental values of the magnetic moments μ_{eff} for pyroborate $\text{Co}_2\text{B}_2\text{O}_5$ ($n_{\text{Co}^{2+}} = 2$) [47], ludwigites $\text{Co}_{2.5}\text{Ti}_{0.5}\text{BO}_5$ [27], and $\text{Co}_{2.5}\text{Sn}_{0.5}\text{BO}_5$ ($n_{\text{Co}^{2+}} = 2.5$) [28], kotoite $\text{Co}_3\text{B}_2\text{O}_6$ ($n_{\text{Co}^{2+}} = 3$) [48], and $\text{Co}_4\text{B}_6\text{O}_{13}$ [49], which contain only Co^{2+} ions as a source of magnetism as a function of the n_{Co} per f.u., as shown in Fig. 8. All of them show the values of μ_{eff} very close to each other and to $4.9 \mu_B/\text{Co}^{2+}$, which corresponds to $g_{\text{Co}^{2+}} \approx 2.5$. The assumption of spin-orbital contribution for Co^{2+} ions with g factor obtained above will change the effective magnetic moment of Co_3BO_5 in two

ways: (i) the moment has a slow increment with the increase in the n_{Co} if Co^{3+} ions are assumed to be in HS state (orange line and values above it); (ii) the moment rapidly decreases if Co^{3+} ions are in LS state (blue line and values below). As can be seen, the magnetic moment of Co_3BO_5 obtained in this paper and in previous studies for a more extended interval $T \leq 300$ K agrees well with the assumption of LS state of Co^{3+} . Moreover, if our assumption is valid, strong ferromagnetism of Co_3BO_5 with magnetic moment $M_r = 3.4(1) \mu_B/\text{f.u.}$ should be attributed to the almost collinear ferrimagnetic ordering of two Co^{2+} moments with $g = 2.5$ that is 0.91 of the expected $M_{\text{sat}} = ngS\mu_B = 3.75 \mu_B/\text{f.u.}$ Thus, one can conclude that, at low temperatures ($T < 300$ K), the value of effective magnetic moment ($5.7 \mu_B/\text{f.u.}$) is compatible with two Co^{2+} ions in the HS state (and some orbital contribution) and the Co^{3+} ions in a LS state. This fact additionally supports the results of neutron powder diffraction that only the Co^{2+} ions are magnetic, and the Co^{3+} ions are in the LS state [29].

Note that, for $\text{Co}_{2.4}\text{Ga}_{0.6}\text{BO}_5$ and $\text{Co}_{2.88}\text{Cu}_{0.12}\text{BO}_5$ ludwigites whose magnetic moments contain the Co^{2+} and a certain amount of Co^{3+} , the μ_{eff} falls into the range of LS values. Qualitatively, both compounds show a behavior like Co_3BO_5 , reflecting a ferrimagnetic ordering of cobalt magnetic moments near 40 K [20, 21], thereby indirectly pointing out the similar nature of Co magnetism in these compounds.

C. DSC

The mass change (TG) and heat flux (DSC) measurements of Co_3BO_5 are shown in Fig. 9. The heating-cooling cycle in air (20% $\text{O}_2 + \text{Ar}$) was performed twice; however, the

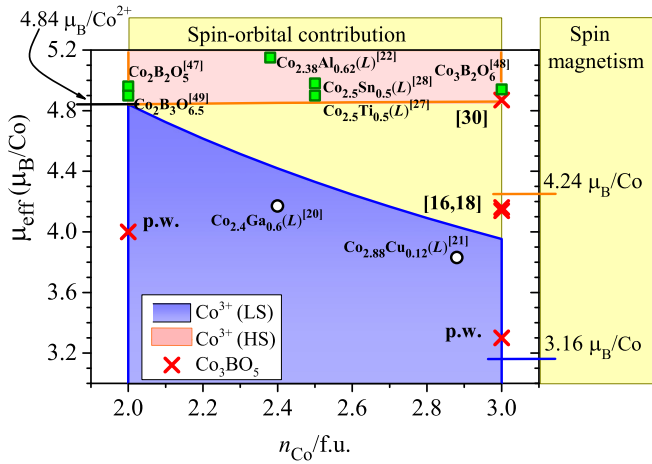


FIG. 8. Magnetic moment of Co-based borates/oxyborates vs number of cobalt ions per formula unit (f.u.; see text). For a better comparability, the magnetic moment data are given per one cobalt ion. The symbol (L) denotes the ludwigite. Right panel shows the values of magnetic moments per Co ion in Co_3BO_5 expected in the spin-only magnetism approximation. The central panel contains the values of magnetic moments, assuming some orbital contribution for HS Co^{2+} ions: the orange line and values above are expected values for the high-spin (HS) Co^{3+} ions, while the blue line and values below are for the low-spin (LS) Co^{3+} ions in the Co-containing ludwigites. The red crosses depict μ_{eff} experimental results, “p.w.” denotes present work. Experimental results: ($n_{\text{Co}}/\text{f.u.} = 2$) under the assumption of only two Co^{2+} ions contributing to magnetism of Co_3BO_5 , ($n_{\text{Co}}/\text{f.u.} = 3$) assuming that all Co ions are contributing to its magnetism.

cooling-heating curves of the second cycle are not shown since they ideally superimpose the corresponding curves of the first cooling-heating cycle. The DSC-TG curves indicate that there are no changes in weight or thermal effects in a wide temperature range 373–773 K. These results show that Co_3BO_5 is thermally stable in the temperature range of interest. Our observation is in strong contradiction with the data of Ref. [30], where two endothermic (exothermic) peaks at

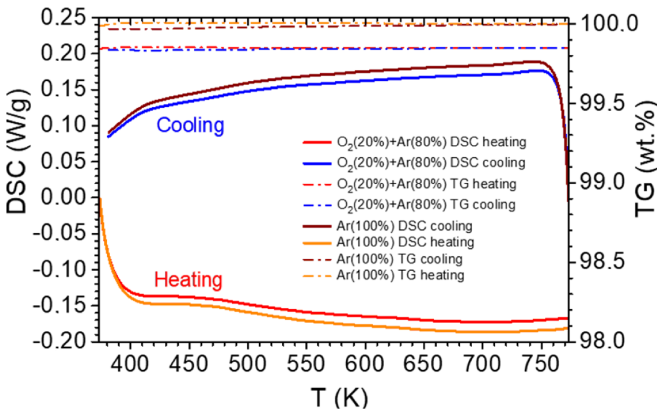


FIG. 9. Differential scanning calorimetry-mass change (DSC-TG) curves (heating-cooling cycles) showing the thermal stability of the Co_3BO_5 powder sample in different gas mixtures: 20 vol.% O_2 in Ar and high pure Ar.

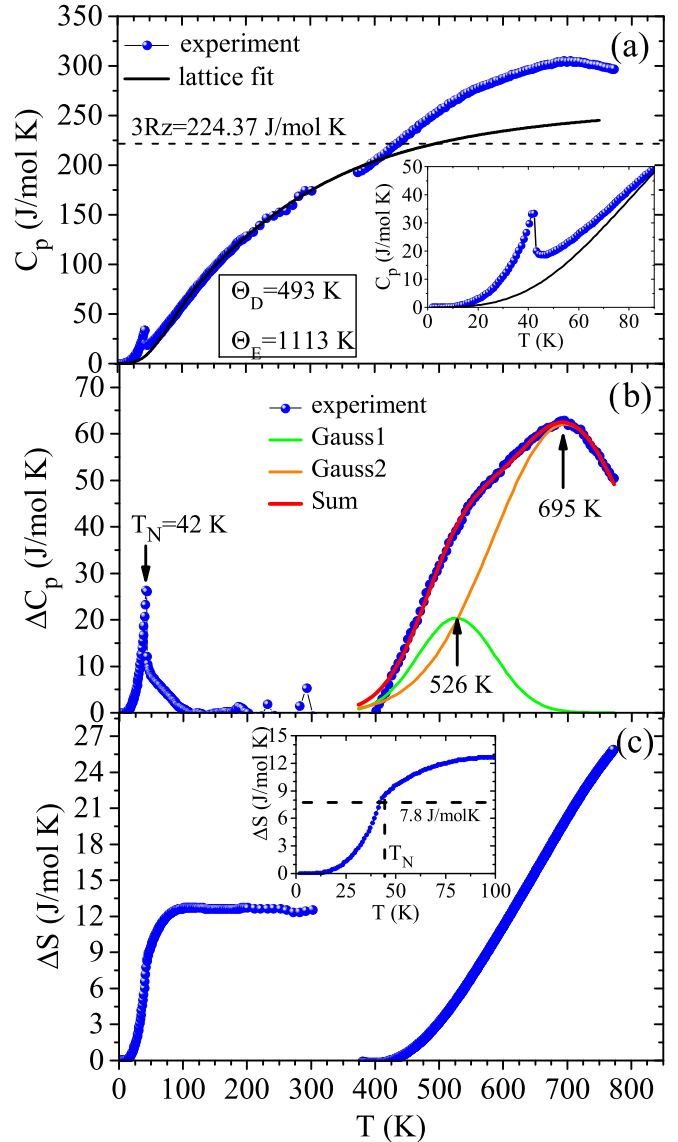


FIG. 10. (a) Temperature dependence of the specific heat in Co_3BO_5 measured from 2 to 300 K and from 373 to 773 K. Dotted line indicates the Dulong-Petit value. The black line refers to a phonon contribution which has been fit to the data well outside the anomaly. Inset: enlarged low-temperature part highlights the onset of ferrimagnetic spin ordering at T_N . (b) The difference of the experimental data and the phonon contribution. Besides the T_N , the arrows show the anomalies in specific heat obtained from the sum of two Gaussians (green and orange). (c) Entropy as a function of temperature. The inset is the range of magnetic phase transition.

472 and 493 K were found under heating (cooling) cycles and assigned to phase transitions.

D. Specific heat capacity

The temperature dependence of the heat capacity taken at $H = 0$ T is shown in Fig. 10(a). At low temperatures, a quite pronounced λ -type anomaly at $T_N = 42$ K implies a second-order phase transition, which is in good agreement with the previously published heat capacity data [16]. In magnetic field, the λ -type anomaly is progressively smeared out and

shifts to higher temperatures (not shown). The above results combined with DSC measurements confirm that the title material does not exhibit a phase transition at high temperatures in contrast to the previous report [30].

For Co_3BO_5 , the thermodynamic limit of the lattice contribution to the entropy $3Rz = 224.37 \text{ J/mol K}$, with $R = 8.314 \text{ J/mol K}$ being the gas constant and $z = 9$ the number of atoms per f.u., is apparently reached at 440 K. Above this temperature, the specific heat C_p shows a significant contribution above the lattice heat capacity, obviously of electronic and/or magnetic origin. To estimate the anomalous contribution of the specific heat ΔC_p , we have fit the main phononic contribution to $C_p(T)$ using Debye-Einstein approximation at temperatures well outside the region of the T_N anomaly. We obtain a reasonable value of Debye temperature $\Theta_D = 493 \pm 20 \text{ K}$. Note, the obtained value is larger than the 140 K found in Ref. [16], but it is in good agreement with the values extracted for other mixed-valence oxyborates Mn_2BO_4 ($\Theta_D = 512 \text{ K}$) [50] and V_2BO_4 ($\Theta_D = 360 \text{ K}$) [51], reflecting the rigid frame of chemical bonds in borate structures.

The anomalous contribution ΔC_p is shown in Fig. 10(b). A significant anomalous contribution besides that at T_N is seen in ΔC_p vs T at elevated temperatures. This quite pronounced anomaly has not a jumplike shape, but a smeared one with a maximum at $\sim 700 \text{ K}$ and a clear shoulder at about 500 K. The best fitting of ΔC_p is obtained by the sum of two Gaussians centered at 526 and 695 K.

The low temperature λ -peak entropy and enthalpy content has been calculated by extrapolating its HC below T_N to a T^3 dependence, as corresponds to the spin-wave contribution of a ferrimagnetic lattice, and above T_N to the high-temperature T^{-2} dependence, yielding the values:

$$(a) \quad 0 < T < T_N, \quad \Delta S/R = 1.00 \pm 0.2, \quad \Delta H/R = 33 \pm 3 \text{ K},$$

$$(b) \quad T_N < T < \text{infinity}, \quad \Delta S/R = 0.7 \pm 0.2, \quad \Delta H/R = 59 \pm 3 \text{ K},$$

and total anomalous values $\Delta S/R = 1.6 \pm 0.2$. We observe in Fig. 10(c) that the anomalous entropy has reached a plateau value already at 100 K. The total enthalpy is $\Delta H/R = 92 \pm 3 \text{ K}$, expressed in gas constant units. The critical entropy, i.e., below T_N , per Co ion is $S_c(\text{Co})/R = 0.50 \pm 0.02$. The entropy above T_N per Co^{2+} , $(S_\infty - S_c)(\text{Co})/R = 0.68/2 = 0.34$, $(S_\infty - S_c)/S_c = 0.68$. The enthalpy is referenced to $U(T = \infty) = 0$, then $(U_\infty - U_o)(\text{Co})/T_N = 1.10$, $(U_\infty - U_c)(\text{Co})/T_N = 0.70$. These values are comparable with those values found in $3d$ Heisenberg antiferromagnets, for example, to the SmGa Garnet [52].

The total anomaly entropy content is provided by the long-range ordering of the magnetic Co^{2+} ions, since the Co^{3+} ions bear no magnetic moment. At this temperature, the compound is an insulator; thus, the Co^{2+} electronic states are governed by crystal field interaction and Co-Co exchange interactions. The former splits the $3d^7$ levels into Kramers doublets, and consequently, its ground state is a Kramers doublet [53,54], with the excited level several hundred K higher energy. Below T_N , the latter exchange interaction further splits the ground doublet upon magnetic ordering. Therefore, the total entropy content expected per ion is $\Delta S_{\text{ion}}/R = \ln 2 = 0.692$. Consequently, the experimental entropy content $\Delta S/R = 1.6 \pm 0.2 = (2.3 \pm 0.2) \ln 2$, indicates that there are about 2.3 Co^{2+}

per f.u. in the Co_3BO_5 compound. Thus, within the experimental error, this result reinforces the conclusion that the $M4$ site is filled mostly by nonmagnetic Co^{3+} , and the other sites are filled by the Co^{2+} ($3d^7$) ions.

E. High-temperature XRD

Several experimental studies of the Co_3BO_5 crystal structure have been performed [6,16,30,38,55]. Most of them consist of a structural characterization at room temperature, and only Refs. [16,30] are devoted to the study of temperature effects. In the latter, the structural properties were studied using high-temperature x-ray powder diffraction. Here, we have performed single-crystal XRD measurements as a function of temperature that allows determining the temperature-driven changes in the bond lengths and the local coordination of the Co ions.

The structure determination was done at 296, 403, 503, 603, and 703 K. No conformation change was observed. The main information about crystal data, data collection, and refinement are reported in Table II. Coordinates of atoms and parameters of isotropic and anisotropic displacements are presented in Tables 1S and 2S, while bond lengths are summarized in Table 3S of the Supplemental Material [56]. The room-temperature lattice parameters are like those found in Refs. [6,16,30,38,55,57]. For better comparability, the structural data obtained in this paper are superimposed on the data from Ref. [30] (Fig. 1S in the Supplemental Material [56]). As can be seen, at room temperature, the a parameter shows a slight decrement compared with the reference data which, however, decreases with temperature. Other lattice parameters are in good agreement with those referred.

Note that, with increasing temperature, all parameters behave similarly to those obtained in Ref. [30], demonstrating that the slope changes at about 500 K. Additionally, the a -lattice parameter shows negative thermal expansion (Fig. 11). With heating, the increase in the volume $\Delta V/V$ reaches a value of 4.5%. The thermal expansion coefficients show an initial linear regime between 300 and 400 K. Above 400 K, the three coefficients (b , c , and volume) rapidly increase, reaching a maximum at about $T_1 = 500 \text{ K}$, and then grow again at $T_2 = 700 \text{ K}$.

Like the lattice parameters, Co-O bond lengths in Co_3BO_5 show an increase with temperature [Fig. 12(a)]. The temperature has a dramatic effect on the Co_2O_6 and especially on the Co_4O_6 octahedra, resulting in the rapid growth of the bond lengths. The mean bond lengths of the Co1 and Co3 sites practically do not change with an increase in the temperature. For the analysis of the local distortions, we used the main component V_{zz} of the $G_{\alpha\beta}$ tensor of the electrical field gradient produced by the different octahedral oxygen coordinations around the individual cobalt sites

$$G_{\alpha\beta} = 2e \sum_i \frac{3\cos^2\varphi_i - 1}{r_i^3}, \quad (3)$$

where φ_i is the angle between the principal octahedra axis and the direction toward the i th oxygen anion, r_i is the distance between the cation and the i th oxygen, and e is the elementary charge [58]. In Fig. 12(b), the main components V_{zz} for different cobalt sites are plotted as a function of

TABLE II. Crystallographic data and main parameters of processing and refinement Co₃BO₅. CIF: the Cambridge Crystallographic Data Centre, Deposition Numbers 2063621–2063625.

Crystal data					
M_r	267.60				
Space group, Z	$Pbam$, 4				
Size, mm	$0.3 \times 0.2 \times 0.1$				
T , K	296	403	503	603	703
a , (Å)	9.2742 (5)	9.2694 (4)	9.2520 (7)	9.2487 (17)	9.2676 (11)
b , (Å)	11.9590 (7)	11.9902 (6)	12.0745 (9)	12.169 (2)	12.2473 (15)
c , (Å)	2.9787 (2)	2.9906 (1)	3.0167 (2)	3.0314 (6)	3.0467 (4)
V , (Å ³)	330.37 (3)	332.38 (2)	337.01 (4)	341.18 (11)	345.81 (7)
D_x , Mg/m ³	5.380	5.348	5.274	5.210	5.140
μ , mm ⁻¹	14.770	14.681	14.479	14.302	14.111
Data collection					
Wavelength	MoK $_{\alpha,\lambda}$ = 0.7106 Å				
Measured reflections	6883	6526	6754	6734	7355
Independent reflections	1058	914	953	938	1073
Reflections with $I > 2\sigma(I)$	848	735	728	715	713
Multiscan					
Absorption correction	Multiscan				
R_{int}	0.0697	0.0736	0.0776	0.0832	0.0968
$2\theta_{max}$ (°)	78.31	72.36	73.04	72.20	75.88
H	-15 → 15	-15 → 15	-15 → 15	-15 → 15	-15 → 15
K	-20 → 20	-19 → 19	-20 → 20	-20 → 20	-21 → 20
L	-5 → 5	-4 → 4	-5 → 5	-5 → 5	-5 → 5
Refinement					
$R[F^2 > 2\sigma(F^2)]$	0.0337	0.0309	0.0305	0.0333	0.0389
$wR(F^2)$	0.0931	0.0657	0.0716	0.0738	0.0837
S	0.823	1.078	1.084	1.107	1.107
Weight	$w = 1/[\sigma^2(F_o^2) + (0.0808P)^2 + 2.653P]$	$w = 1/[\sigma^2(F_o^2) + (0.0244P)^2 + 0.644P]$	$w = 1/[\sigma^2(F_o^2) + (0.03214P)^2 + 0.380P]$	$w = 1/[\sigma^2(F_o^2) + (0.0280P)^2 + 0.513P]$	$w = 1/[\sigma^2(F_o^2) + (0.0333P)^2 + 0.796P]$
	where $P = \max(F_o^2 + 2F_c^2)/3$				
Extinction	0.039 (3)	0.040 (2)	0.044 (2)	0.045 (3)	0.054 (3)
$(\Delta/\sigma)_{max}$	<0.001	<0.001	<0.001	<0.001	<0.001
$\Delta\rho_{max}$, e/Å ³	2.343	1.687	1.468	2.343	2.420
$\Delta\rho_{min}$, e/Å ³	-0.817	-1.243	-1.258	-0.817	-1.411

temperature. To begin with, we consider the local distortions at room temperature. The Co²⁺ ions at the Co1 and Co3 sites have a coordination, forming axially compressed octahedra and, thus, showing the largest values of V_{zz} . Although the Co2O₆ shows axial compression, it is much less than that for Co1O₆ and Co3O₆. Here, Co4O₆ octahedron has two short (equatorial) Co4-O1, two long (equatorial) Co4-O4, and two intermediate (axial) Co4-(O2)O3 bonds, thereby showing a slight axial elongation. The coordination bond lengths seem to be more homogeneous around Co4, making it the most regular octahedron with the smallest $V_{zz}(4)$.

The difference in the local deformations arises from different boron coordination. As it is seen from Fig. 13 for Co1 and Co3 sites, four oxygen atoms in the equatorial plane (O3 for Co1 and O2, O5 for Co3) participate in short B-O bonds, resulting in considerable elongation of appropriate bonds.

However, there are only two oxygen atoms coordinated with the boron atoms in the case of the Co2O₆ and Co4O₆ octahedra (O5 for Co2 and O2, O3 for Co4), also causing elongation of the Co4-O bond in direction of the (BO₃)³⁻ groups. It must be mentioned that the compression of the Co2O₆ octahedron along Co2-O5 bonds is not in line with the expected distortion. The source of this discrepancy is probably the O4 atom in the equatorial plane, which is the bridge between Co2 and Co4 atoms and participates in the simultaneous compression of the Co2-O4 and the stretching of Co4-O4 bonds. This oxygen atom has relative freedom for the displacement, which facilitates the entering of the substitution atoms (Cu, Fe, Mn, Ga, Al) into the 4-2-4 triad [20–23,26].

Heating the sample above 400 K triggers a stretching of equatorial Co3-O bonds and, thus, indirectly a compression of equatorial Co1-O ones inside the 3-1-3 triad. In addition, there is an elongation of the axial Co1-O bonds. As a result,

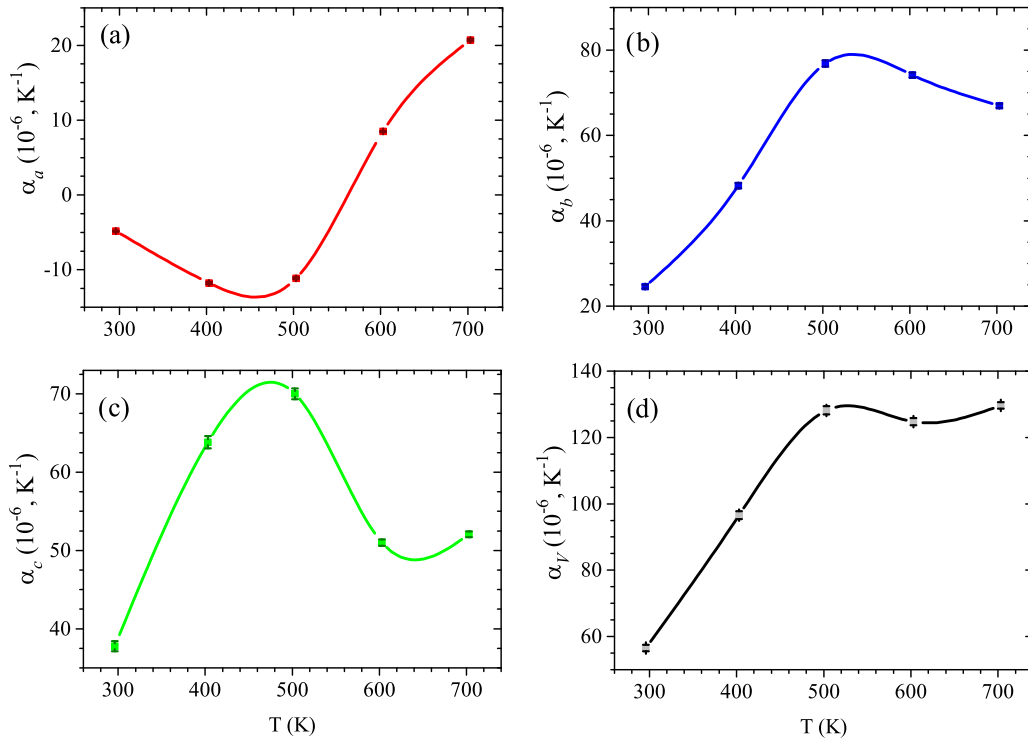


FIG. 11. Temperature dependence of the expansion coefficients: (a) a parameter, (b) b parameter, (c) c parameter, and (d) unit cell volume.

the Co1O_6 becomes more regular, while the Co3O_6 shows the opposite tendency. The other subsystem formed by Co^{2+} and Co^{3+} in sites 2 and 4 behaves in a different way. The local distortion of the Co4 site rises while the $V_{zz}(2)$ for Co^{2+} ions sharply drops. As a result, the difference in the octahedral environments of two metal sites decreases and becomes negligible at 703 K. The careful analysis of the Co4O_6 bond lengths has revealed that the axial bonds, directed along BO_3 groups, grow much faster than equatorial ones, resulting in dramatic changes in V_{zz} (Fig. 2S in the Supplemental Material [56]).

The room-temperature oxidation states evaluated using a bond-valence-sum approach (BVS) [59] suggest that the Co1,

Co2, and Co3 sites are occupied by the Co^{2+} ions, whereas the Co4 site is filled by Co^{3+} (atomic charges 2.78(6)/2.84(7) when bond valence parameters are related to $\text{Co}^{2+}/\text{Co}^{3+}$ oxidation state; Table 3S in the Supplemental Material [56]). The empirical estimates of the valence for the boron site are consistent with +3. Thus, the BVS calculations clearly indicate the localized character of $3d$ electrons at all metal sites, highlighting the charge ordering at room temperature.

The electron count in a triad 4-2-4 corresponds to three Co^{3+} ions with one extra electron per triad. This itinerant electron could be localized at the Co2 site, smeared over all three sites, or distributed between two adjacent Co2-Co4 sites, leading to the dimerization state. In the Fe_3BO_5 , a dimer

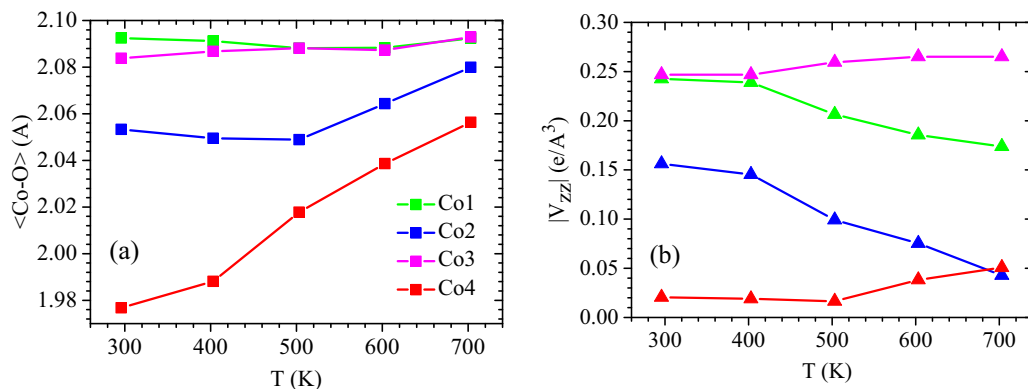


FIG. 12. (a) Temperature dependences of mean bond lengths and (b) main components of the electrical field gradient in Co_3BO_5 .

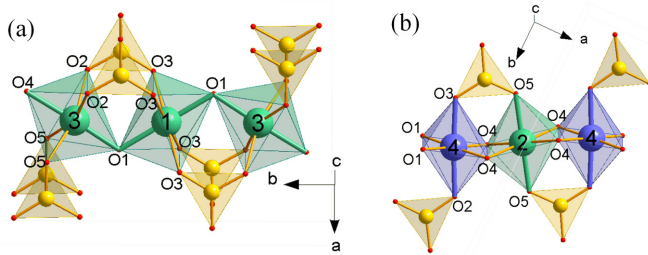


FIG. 13. The metal and boron coordination in Co_3BO_5 ludwigite. The triads (a) $\text{Co}_3\text{-Co1-Co}_3$ and (b) $\text{Co}_4\text{-Co2-Co}_4$ formed by divalent and trivalent ions are shown. The main octahedral axes along which the compression or elongation is observed are highlighted in bold.

formation at the 4-2-4 ladder is associated with a structural phase transition and change in space group from $Pbam(\text{No}55)$ to $Pbnm(\text{No}62)$ at $T_{\text{ST}} = 283$ K [9,10]. However, in Co_3BO_5 , neither present nor previous XRD studies reveal any structural phase transition over all investigated temperatures, confirming the absence of the dimerization of the 4-2-4 triad in this compound.

The thermal expansion coefficients of b , c , and unit cell have nonmonotonic dependence on the temperature, going through a maximum at $T_1 = 500$ K, where heat capacity and conductivity show the anomalies. This correlates with a rapid increase in the octahedral Co-O distances at the Co_4 site, occupied by Co^{3+} , and points out a manifestation of another mechanism of lattice expansion besides the conventional lattice anharmonicity. This mechanism can be attributed to the spin fluctuations arising from the change in the ionic radius of the Co^{3+} ion at spin-state transition from LS to HS.

It is instructive to compare the LS-HS transition of the Co^{3+} ion discussed here with simpler perovskite rare-earth cobaltites LnCoO_3 ($\text{Ln} = \text{La, Dy, Sm, Gd, \dots}$) (Refs. [60–62] and herein). In LaCoO_3 , a spin-state transition is well known and reveals itself with a sharp peak in the magnetic susceptibility at 150 K and smooth metallization above 500 K [63,64]. The maximum thermal expansion coefficient results from strong thermal fluctuations of the Co^{3+} ions multiplicity between the LS and HS terms. All thermodynamic properties, including the thermal expansion, magnetic susceptibility, and specific heat are correlated with the spin-state transition in rare-earth cobaltites [65]. Moreover, maxima in the thermal expansion and magnetic susceptibility are related to the maximal rate of the multiplicity fluctuations when the derivative of the concentration of thermally excited HS terms dn_{HS}/dT has a maximum.

This comparison indicates that, in the Co_3BO_5 , the maximal rate of the multiplicity fluctuations occurs at the temperature close to $T_1 = 500$ K. In addition, the comparison of the ionic radii of the Co^{3+} ion at HS (0.61 Å) and LS states (0.545 Å) gets the difference of about 0.07 Å [66]. This value matches well with the change in the average $\text{Co}_4\text{-O}$ distance (0.08 Å) > 500 K and is a clear hint of the spin-state crossover. Using the same methodology as for perovskite-like cobaltites, the second anomaly observed in the temperature dependences of the expansion coefficients and the heat capacity with the maximum at $T_2 = 700$ K can be associated with the smooth electronic transition caused by the modification of electronic

structure. The conductivity data on Co_3BO_5 presented in Ref. [30] shows a gradual increase in $\sigma(T)$ up to the highest measured temperature of 505 K. The electrical measurement data at elevated temperatures are not currently available.

Note that we have observed negative thermal expansion of the a parameter in another homometallic oxyborate Mn_2BO_4 within the same T interval (300–500 K) [67]. The warwickites and ludwigites have strong structural affinities and belong to the “3 Å wall-paper structures.” In both compounds, the planar BO_3 triangles parallel to the (110) plane connect adjacent layers of metal ions in the [100] direction by corner-sharing. In ludwigites, M_4 sites located in the voids between the BO_3 tunnels are filled by M^{3+} ions, whereas in warwickites, similar sites are occupied by both divalent and trivalent ions. From the crystal-chemical background, it can be expected that these structures should be more rigid in the a direction due to the rigidity of the bonds within the BO_3 group and that the thermal or substitution effects should be more pronounced in the b and c directions. This is confirmed by the comparison of values of thermal expansion coefficients for both materials. Therefore, we can assume that the observed anomalies of a parameters result from the structural peculiarities of the related oxyborates.

Focusing on the available structural data on the Co-based ludwigites and taking the mean bond length $\langle \text{Co-O} \rangle$ as a size of a given CoO_6 octahedron, we have estimated the influence of the temperature and the cation size on the crystal structure. We checked the dependence of the lattice parameters and cell volume on the effective ion radius of metal ions (r_i) located at different sites M_1 , M_2 , M_3 , and M_4 and found that only the size of the M_4 site causes a monotonic change in the crystal parameters. The larger the r_i at the M_4 site, the larger the lattice parameters [Figs. 14(a)–14(c)]. The c parameter and the unit cell volume show almost linear dependence on the r_i [Figs. 14(c) and 14(d)], which demonstrates a regular linear increase with the effective radius of the metal ion located at the M_4 site [in Fig. 14(d)]. The use of the linear fit allows us to predict the cell volume of Co_3BO_5 in the case when the M_4 site is occupied by the LS instead of the HS Co^{3+} ions [see bottom labels in Fig. 14(d)]. The volumes defined in this way were found to be $\sim 325.9 \pm 4.2$ and $340.1 \pm 3.9 \text{ \AA}^3$ for LS and HS, respectively, which corresponds to the change $\Delta V/V$ of about 4.4%, very close to that experimentally observed. The substitution of a smaller Co^{3+} ion for larger Ga^{3+} , Mn^{3+} , Fe^{3+} , $\text{Co}^{2+}/\text{Ti}^{4+}$, and $\text{Co}^{2+}/\text{Sn}^{4+}$ modifies the structural properties in the same way as the thermal expansion of pure Co_3BO_5 > 500 K. This conclusion is suitable for all Co-substituted ludwigites and clearly indicates the crucial role of the M_4 ion in long-range crystal structure.

The second conclusion is that there is a minimum a -axis length over which the ludwigite structure is stable. The lack of compressibility $< 9.24 \text{ \AA}$ is likely due to the incompressibility (and stiffness to resist thermal expansion) of the BO_3 triangles. This stiffness does not affect either the c axis (due to connectivity differences) or the b axis (due to its ability to absorb the compression through the buckling of the corner-sharing octahedra connections). This incompressibility of the structure in the a -axis direction is probably the cause for the Co^{3+} cation in the M_4 site to be in LS state at room temperature, despite the HS configuration being normally

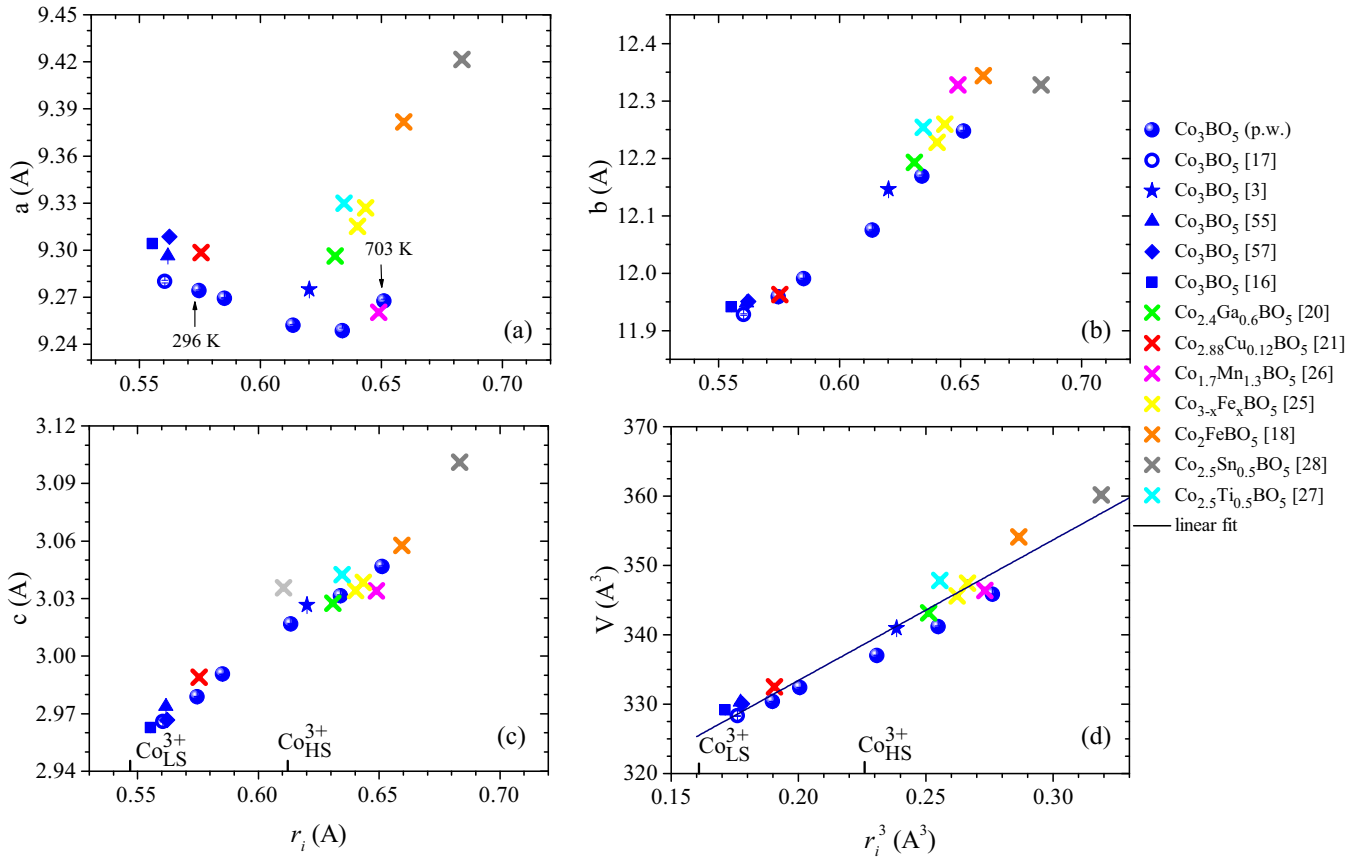


FIG. 14. (a)–(c) a , b , and c lattice parameters presented as a function of the effective ion radius (r_i) at the M4 site and (d) unit cell volume vs r_i^3 . The bottom labels of (c) and (d) show the effective ionic radii of Co^{3+} at low-spin (LS) and high-spin (HS) states according to Shannon [66].

favored since this reduces the ion size. When the structure expands because of thermal expansion (or partial substitution on the M4 site), the larger HS Co^{3+} ion can fit in without causing conflicts with the bonding requirements of the BO_3 triangles.

Finally, the data on pure Co_3BO_5 reported by different groups and earlier by our group demonstrate some difference in the lattice parameters, though remaining in the general trend. These features of the crystal structure may reflect the influence of the synthesis technique, as well as the technological factors within the same technique, for example, the flux one. Although, the magnetic properties of the samples (the magnetic moment, temperature of magnetic transition, etc.) [16,18,30] differ little, they can somewhat determine the electronic properties of the compound and lead to difference in the crystal's behavior (for example, phase transitions seen in DSC in Ref. [30] but not in this paper). The cationic distribution and different degree of ordering due to different thermal history may be also affected. The Cu_2Fe [68,69] and Co_2Al [22,23] ludwigites can be considered as examples, where the Fe^{3+} and Al^{3+} ions are differently distributed over nonequivalent metal sites, leading to difference in electronic and magnetic behavior. The influence of the cation distribution requires additional study, as it was done for rare-earth ferrobates [70].

F. Results of the DFT + U calculations

To understand the obtained results and determine the magnetic and electronic structure of Co_3BO_5 , complementary theoretical studies have been carried out. The calculations were done using the GGA + U approach for both low- and high-temperature phases. For this, the crystal structures corresponding to $T = 296$ and 703 K, respectively, obtained in our XRD experiments and magnetic structure determined in Ref. [29] were utilized.

Thanks to the ability of the GGA + U approach to stabilize different solutions corresponding not only to the global, but also different local minima of the density functional, we calculated total energies of two configurations, where the Co4 ion is either magnetic or not (these configurations were obtained in conventional self-consistent DFT + U calculations without any constraints). These configurations are dubbed as $\downarrow\uparrow\uparrow\downarrow$ or $\downarrow\uparrow\uparrow 0$, where \uparrow stands for spin up and \downarrow for spin down, and the order of signs corresponds to labels of the Co ions.

We found that the low temperature phase $\downarrow\uparrow\uparrow 0$ configuration with nearly nonmagnetic Co4 ions has the lowest total energy, while the $\downarrow\uparrow\uparrow\downarrow$ solution is 46.88 meV per cell (12 Co ions) or 11.72 meV per Co4 ion higher in energy. Considering that the calculations were performed for the structure corresponding to $T = 296$ K, one may expect that this con-

TABLE III. Magnetic moment (μ_B) of Co ions in Co_3BO_5 obtained for high- and low-temperature phases in the GGA + U calculations.

	Room (low) T phase		High T phase	
	$\downarrow\uparrow\uparrow\downarrow$	$\downarrow\uparrow\uparrow 0$	$\downarrow\uparrow\uparrow\downarrow$	$\downarrow\uparrow\uparrow 0$
Co1	2.8	2.8	2.8	2.8
Co2	2.8	2.7	2.8	2.8
Co3	2.8	2.8	2.8	2.8
Co4	3.2	0.2	2.6	0.2

figuration can be thermally excited at temperatures ~ 432 K, i.e., close to the first anomaly in unit cell parameters observed experimentally.

Careful analysis of the occupation matrixes shows that there is a charge ordering in this low-temperature phase: Co1, Co2, and Co3 are $2+$ and have $3d^7$ electronic configuration, while Co4 is $3+$ with six $3d$ electrons in both solutions. Moreover, the Co4 ion is in the LS state in $\downarrow\uparrow\uparrow 0$ and the HS state in the $\downarrow\uparrow\uparrow\downarrow$ configuration. A list of magnetic moments on each Co ion can be found in Table III. The density of states plots for both configurations are shown in Fig. 15. One may see that the system is insulating with the band gap of 1.4 eV for the $\downarrow\uparrow\uparrow 0$ configuration corresponding the ground state. This is rather important since the spin-state transition by itself does not lead to the metal-insulator transition. As we will show below, only breaking of the charge ordering results in formation of a metallic state. The obtained value of the insulating gap is in reasonably good agreement with the exper-

imental value of $E_g = 2E_a \approx 1.7$ eV previously found from conductivity measurements below room temperature [71].

On the other hand, we see that the charge ordering is not sensitive to the spin state of the Co4 ion: in both calculated configurations, this ion adopts $3+$ charge state. Moreover, we performed additional calculations of other magnetic structures and obtained that, even in fully ferromagnetic state, the Co4 ions are in $3d^6$ electronic configuration. Thus, we see that the mechanism of charge disproportionation is related to features of the crystal structure.

As it has been explained above, local surroundings of the Co1 and Co3 are very different from Co2 and Co4. There are four O^{2-} ions having bonds with B^{3+} ions for Co1 and Co3 ions, but only two for Co2 and Co4. Then the effective electrostatic field acting on Co1 and Co3 is weaker, and already from these geometrical arguments, one may expect that average Co-O distances for these ions should be longer than for Co2 and Co4 and, thus, Co1 and Co3 are prone to be $2+$. This type of reasoning fully agrees with actual experimental Co-O bond distances presented in Fig. 12. From the same Fig. 12, we see that this is the Co4 ion, which has the smallest average Co-O bond length and may adopt $3+$ charge state, for which the ionic radius (for any spin-state) is less than the one of Co^{2+} ions.

However, with increase of the temperature, the difference between average Co-O bond distances for different Co ions nearly vanishes, destabilizing charge ordering. Our GGA + U calculations for the high-temperature phase show that the charge ordering does disappear, all Co ions have $3d^7$ electronic configuration, and the system becomes metallic in the $\downarrow\uparrow\uparrow\downarrow$ configuration (see Fig. 15), which now has the lowest total energy. This finding could reasonably explain

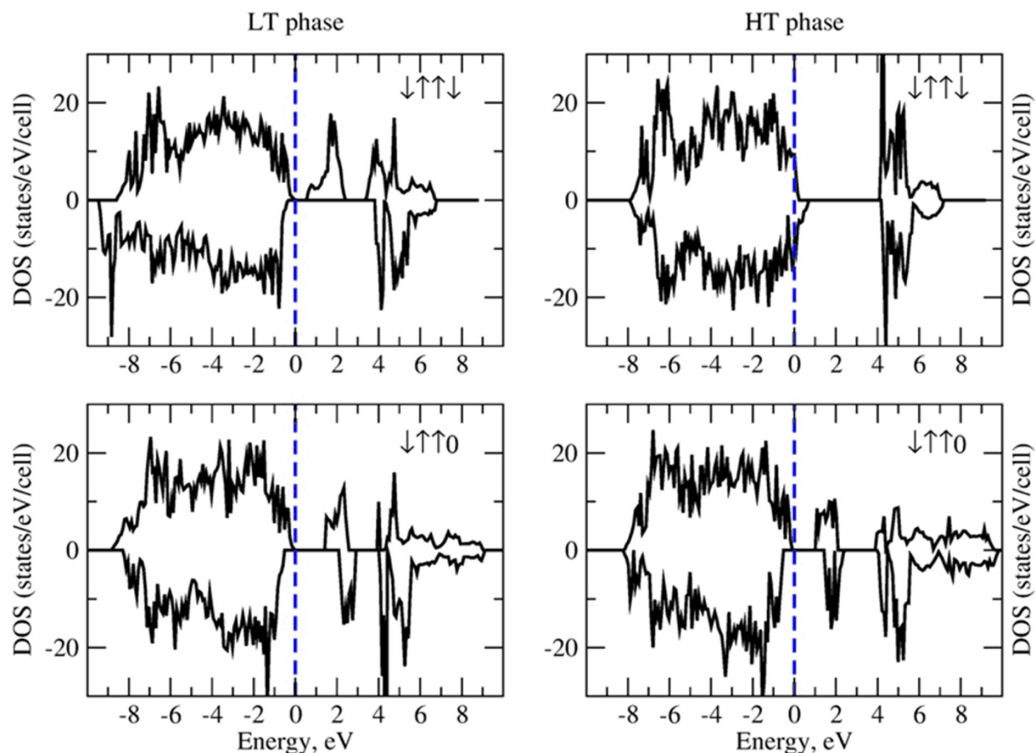


FIG. 15. Co_3BO_5 total density of states for low-temperature and high-temperature phases.

the observed effective moment $\mu_{\text{eff}} = 4.87 \mu_B$ extracted from high-temperature range $T = 500\text{--}700$ K [30]. Indeed, if it is assumed that, at high temperatures, all cobalt ions become divalent $n_{\text{Co}^{2+}} = 3$ and have some orbital moment inherent in Co^{2+} , then $\mu_{\text{eff}} = 4.84 \mu_B/\text{Co}^{2+}$ (left panel of Fig. 8). It must be mentioned that, with given chemical formula, one cannot have an insulating state with all Co ions being $2+$, while in the case of metal, this is possible. However, if such a state will be probed by, e.g., x-ray spectroscopy, then numerous ligand holes should be observed, compensating $2+$ valence state.

IV. CONCLUSIONS

We have studied the electronic and magnetic state of single-crystalline Co_3BO_5 using XMCD, magnetic susceptibility, XRD, DSC, and heat capacity measurements. The experiments were done in a wide temperature interval covering both magnetically ordered and paramagnetic phases. The Co K -edge XANES/XMCD experiments were performed in a ferrimagnetic state. The extracted XANES $_{\text{Co}^{3+}}$ spectrum at low temperature is experimental evidence of the Co^{3+} ions in Co_3BO_5 . The Co sublattice magnetism has a similarity in two isostructural compounds Co_3BO_5 and Co_2FeBO_5 ; in the latter, the Co^{3+} ions are replaced by Fe^{3+} ones. The rather small contribution from the Co^{3+} ion to the XMCD signal of Co_3BO_5 is indicative of the LS state of this ion. The Co and Fe K -edges XMCD measurements recorded in the Co_2FeBO_5 single crystal have uncovered an antiferromagnetic coupling between the two sublattices, which indicates the generality of the formation of magnetic structures in Co_3BO_5 and Co_2FeBO_5 , namely the ferrimagnetic arrangement of Co^{2+} moments and antiferromagnetic arrangement of their moment relative to the magnetic moment at the $M4$ site. The sample-oriented measurements of magnetic susceptibility have revealed that a magnetic behavior of Co_3BO_5 in the paramagnetic regime ($T < 300$ K) is dominated by the high uniaxial anisotropy. Below that temperature, the average effective magnetic moment $5.7 \mu_B/\text{f.u}$ is compatible with two Co^{2+} ions in the HS state and orbital contribution and Co^{3+} in the LS state.

Our measurements of the thermodynamic properties of Co_3BO_5 have explored two anomalies at $T_1 \approx 500$ and $T_2 \approx 700$ K besides the magnetic phase transition at T_N . In contrast to Ref. [30], the high-temperature anomalies we observed in Co_3BO_5 are smooth, which indicates that they are not first- or second-order phase transitions. In line with this finding, our DSC study of the single crystal heated up to 770 K confirmed that the sample is thermally stable. These anomalies detected by heat-capacity also manifested themselves in the XRD measurement, which reveals well-defined maxima of thermal expansion coefficients. We also observed a remarkable sensitivity of the Co4 octahedral site to the temperature effect consisting of a rapid increase in the octahedral Co-O distances and the local distortion (V_{zz}). These changes correlate with the evolution of the Co^{3+} ion in the spin-state crossover > 500 K.

Additionally, the GGA + U calculations show that, at the low-temperature phase, the Co_3BO_5 is an insulator with the band gap of 1.4 eV, the ground state is ferrimagnetic with the Co^{3+} ion being in LS state. Above 500 K, there is a progressive disappearance of charge ordering, all Co ions have $3d^7$ electronic configuration, and the system becomes metallic.

ACKNOWLEDGMENTS

We acknowledge many inspirational discussions on the topic of this paper with the late Natalia Ivanova and Leonard Bezmaternykh. The authors acknowledge A. Ney for allowing us to use the XANES spectrum of ZnCo_2O_4 film. We are grateful to the Russian Foundation for Basic Research (Project No. 20-02-00559) and President Council on Grants (Project No. MK-2339.2020.2) for supporting this paper. This paper was carried out within the state assignment of the Russian Ministry of Science and High Education via program “Quantum” (No. AAAA-A18-118020190095-4). We also acknowledge support by Russian Ministry of Education and Science via Contract No. 02.A03.21.0006. We acknowledge financial support from the Spanish Ministry of Economy, Industry and Competitiveness (MINECO, Grant No. MAT2017-83468-R) and from the regional Government of Aragon (E12-20R RASMIA project).

- [1] J. B. Goodenough, An interpretation of the magnetic properties of the perovskite-type mixed crystals $\text{La}_{1-x}\text{Sr}_x\text{CoO}_{3-x}$, *J. Phys. Chem. Solids* **6**, 287 (1958).
- [2] R. B. Guimaraes, M. Mir, J. C. Fernandes, M. A. Continentino, H. A. Borges, G. Cernicchiaro, M. B. Fontes, D. R. S. Candela, and E. Baggio-Saitovitch, Cation-mediated interaction and weak ferromagnetism in $\text{Fe}_3\text{O}_2\text{BO}_3$, *Phys. Rev. B* **60**, 6617 (1999).
- [3] R. Norrestam, K. Nielsen, I. S¸tofte, and N. Thorup, Structural investigation of two synthetic oxyborates: the mixed magnesium-manganese and the pure cobalt ludwigites, $\text{Mg}_{1.93}\text{Mn}_{1.07}\text{O}_2\text{BO}_3$ and $\text{Co}_3\text{O}_2\text{BO}_3$, *Z. Kristallogr.* **189**, 33 (1989).
- [4] N. B. Ivanova, A. D. Vasil’ev, D. A. Velikanov, N. V. Kazak, S. G. Ovchinnikov, G. A. Petrakovskii, and V. V. Rudenko, Magnetic and electrical properties of cobalt oxyborate Co_3BO_5 , *Phys. Solid State* **49**, 651 (2007).
- [5] J. C. Fernandes, R. B. Guimaraes, M. A. Continentino, H. A. Borges, A. Sulpice, J. L. Tholence, J. L. Siqueira, L. I. Zawislak, J. B. M. Da Cunha, and C. A. Dos Santos, Magnetic interactions in the ludwigite $\text{Ni}_2\text{FeO}_2\text{BO}_3$, *Phys. Rev. B* **58**, 287 (1998).
- [6] R. Norrestam, M. Kritikos, K. Nielsen, I. S¸tofte, and N. Thorup, Structural characterizations of two synthetic Niludwigites, and some semiempirical EHTB calculations on the ludwigite structure type, *J. Solid State Chem.* **111**, 217 (1994).
- [7] M. Onoda, Crystal structure and electronic state of the disordered $S = 1$ system $(\text{Li}_x\text{V}_{1-x})_3\text{BO}_5$ with $x \approx 0.3$, *J. Solid State Chem.* **141**, 418 (1998).
- [8] J. C. Fernandes, R. B. Guimares, M. A. Continentino, L. Ghivelder, and R. S. Freitas, Specific heat of $\text{Fe}_3\text{O}_2\text{BO}_3$: evidence for a Wigner glass phase, *Phys. Rev. B* **61**, R850 (2000).
- [9] M. Mir, R. B. Guimares, J. C. Fernandes, M. A. Continentino, A. C. Doriguetto, Y. P. Mascarenhas, J. Ellena, E. E. Castellano,

- R. S. Freitas, and L. Ghivelder, Structural Transition and Pair Formation in $\text{Fe}_3\text{O}_2\text{BO}_3$, *Phys. Rev. Lett.* **87**, 147201 (2001).
- [10] M. Mir, J. Janczak, and Y. P. Mascarenhas, X-ray diffraction single-crystal structure characterization of iron ludwigite from room temperature to 15 K, *J. Appl. Cryst.* **39**, 42 (2006).
- [11] A. P. Douvalis, A. Moukarika, T. Bakas, G. Kallias, and V. Papaefthymiou, Mössbauer and magnetization studies of Fe_3BO_5 , *J. Phys.: Condens. Matter.* **14**, 3303 (2002).
- [12] J. Larrea J., D. R. Sánchez, F. J. Litterst, E. M. Baggio-Saitovitch, J. C. Fernandes, R. B. Guimarães, and M. A. Continentino, Magnetism and charge ordering in $\text{Fe}_3\text{O}_2\text{BO}_3$ studied by ^{57}Fe Mössbauer spectroscopy, *Phys. Rev. B* **70**, 174452 (2004).
- [13] J. P. Attfield, J. F. Clarke, and D. A. Perkins, Magnetic and crystal structures of iron borates, *Physica B* **180–181**, 581 (1992).
- [14] P. Bordet and E. Suard, Magnetic structure and charge ordering in Fe_3BO_5 : A single-crystal x-ray and neutron powder diffraction study, *Phys. Rev. B* **79**, 144408 (2009).
- [15] J. Bartolomé, A. Arauzo, N. V. Kazak, N. B. Ivanova, S. G. Ovchinnikov, Yu. V. Knyazev, and I. S. Lyubutin, Uniaxial magnetic anisotropy in $\text{Co}_{2.25}\text{Fe}_{0.75}\text{O}_2\text{BO}_3$ compared to $\text{Co}_3\text{O}_2\text{BO}_3$ and $\text{Fe}_3\text{O}_2\text{BO}_3$ ludwigites, *Phys. Rev. B* **83**, 144426 (2011).
- [16] D. C. Freitas, M. A. Continentino, R. B. Guimaraes, J. C. Fernandes, J. Ellena, and L. Ghivelder, Structure and magnetism of homometallic ludwigites: $\text{Co}_3\text{O}_2\text{BO}_3$ versus $\text{Fe}_3\text{O}_2\text{BO}_3$, *Phys. Rev. B* **77**, 184422 (2008).
- [17] N. V. Kazak, N. B. Ivanova, O. A. Bayukov, S. G. Ovchinnikov, A. D. Vasiliev, V. V. Rudenko, J. Bartolomé, A. Arauzo, and Yu. V. Knyazev, The superexchange interactions in mixed Co-Fe ludwigite, *J. Magn. Magn. Mater.* **323**, 521 (2011).
- [18] N. B. Ivanova, N. V. Kazak, Yu. V. Knyazev, D. A. Velikanov, L. N. Bezmaternykh, S. G. Ovchinnikov, A. D. Vasiliev, M. S. Platonov, J. Bartolomé, and G. S. Patrin, Crystal structure and magnetic anisotropy of ludwigite $\text{Co}_2\text{FeO}_2\text{BO}_3$, *J. Exp. Theor. Phys.* **113**, 1015 (2011).
- [19] N. B. Ivanova, M. S. Platonov, Yu. V. Knyazev, N. V. Kazak, L. N. Bezmaternykh, E. V. Eremin, and A. D. Vasiliev, Spin-glass magnetic ordering in $\text{CoMgGaO}_2\text{BO}_3$ ludwigite, *Low Temp. Phys.* **38**, 172 (2012).
- [20] N. B. Ivanova, M. S. Platonov, Yu. V. Knyazev, N. V. Kazak, L. N. Bezmaternykh, A. D. Vasiliev, S. G. Ovchinnikov, and V. I. Nizhankovskii, Effect of the diamagnetic dilution on the magnetic ordering and electrical conductivity in the $\text{Co}_3\text{O}_2\text{BO}_3:\text{Ga}$ ludwigite, *Phys. Solid State* **54**, 2212 (2012).
- [21] N. B. Ivanova, N. V. Kazak, Yu. V. Knyazev, D. A. Velikanov, A. D. Vasiliev, L. N. Bezmaternykh, and M. S. Platonov, Structure and magnetism of copper-substituted cobalt ludwigite $\text{Co}_3\text{O}_2\text{BO}_3$, *Low Temp. Phys.* **39**, 709 (2013).
- [22] C. P.C. Medrano, D. C. Freitas, E. C. Passamani, C. B. Pinheiro, E. Baggio-Saitovitch, M. A. Continentino, and D. R. Sanchez, Field-induced metamagnetic transitions and two-dimensional excitations in ludwigite $\text{Co}_{4.76}\text{Al}_{1.24}(\text{O}_2\text{BO}_3)_2$, *Phys. Rev. B* **95**, 214419 (2017).
- [23] J. Kumar, S. N. Panja, D. J. Mukkattukavil, A. Bhattacharyya, A. K. Nigam, and S. Nair, Reentrant superspin glass state and magnetization steps in the oxyborate Co_2AlBO_5 , *Phys. Rev. B* **95**, 144409 (2017).
- [24] D. C. Freitas, M. A. Continentino, R. B. Guimaraes, J. C. Fernandes, E. P. Oliveira, R. E. Santelli, J. Ellena, G. G. Eslava, and L. Ghivelder, Partial magnetic ordering and crystal structure of the ludwigites $\text{Co}_2\text{FeO}_2\text{BO}_3$ and $\text{Ni}_2\text{FeO}_2\text{BO}_3$, *Phys. Rev. B* **79**, 134437 (2009).
- [25] N. V. Kazak, Yu. V. Knyazev, M. S. Platonov, A. O. Vasiliev, L. N. Bezmaternykh, V. V. Rudenko, N. B. Ivanova, J. Bartolome, A. Arauzo, and S. G. Ovchinnikov, Electronic and magnetic states of the Co and Fe in ludwigite system $\text{Co}_{3-x}\text{Fe}_x\text{BO}_5$, in *Proceedings of the VII Euro-Asian Symposium "Trends in Magnetism,"* Ekaterinburg, Russia (2019).
- [26] Yu. V. Knyazev, N. B. Ivanova, N. V. Kazak, M. S. Platonov, L. N. Bezmaternykh, D. A. Velikanov, A. D. Vasiliev, S. G. Ovchinnikov, and G. Yu. Yurkin, Crystal structure and magnetic properties of Mn substituted ludwigite $\text{Co}_3\text{O}_2\text{BO}_3$, *J. Magn. Magn. Mater.* **324**, 923 (2012).
- [27] D. C. Freitas, R. B. Guimarães, D. R. Sanchez, J. C. Fernandes, M. A. Continentino, J. Ellena, A. Kitada, H. Kageyama, A. Matsuo, K. Kindo, G. G. Eslava, and L. Ghivelder, Structural and magnetic properties of the oxyborate $\text{Co}_5\text{Ti}(\text{O}_2\text{BO}_3)_2$, *Phys. Rev. B* **81**, 024432 (2010).
- [28] C. P.C. Medrano, D. C. Freitas, D. R. Sanchez, C. B. Pinheiro, G. G. Eslava, L. Ghivelder, and M. A. Continentino, Nonmagnetic ions enhance magnetic order in the ludwigite $\text{Co}_5\text{Sn}(\text{O}_2\text{BO}_3)_2$, *Phys. Rev. B* **91**, 054402 (2015).
- [29] D. C. Freitas, C. P.C. Medrano, D. R. Sanchez, M. Nunez Regueiro, J. A. Rodríguez-Velamazán, and M. A. Continentino, Magnetism and charge order in the ladder compound $\text{Co}_3\text{O}_2\text{BO}_3$, *Phys. Rev. B* **94**, 174409 (2016).
- [30] C. W. Galdino, D. C. Freitas, C. P.C. Medrano, R. Tartaglia, D. Rigitano, J. F. Oliveira, A. A. Mendonça, L. Ghivelder, M. A. Continentino, D. R. Sanchez, and E. Granado, Magnetic, electronic, structural, and thermal properties of the $\text{Co}_3\text{O}_2\text{BO}_3$ ludwigite in the paramagnetic state, *Phys. Rev. B* **100**, 165138 (2019).
- [31] G. M. Sheldrick, A short history of SHELX, *Acta Crystallogr. Sect. A* **64**, 112 (2008).
- [32] G. M. Sheldrick, *SHELXS and SHELXL97. Program for Crystal Structure Refinement* (University of Göttingen, Germany, 1997).
- [33] G. Kresse and J. Furthmüller, Efficient iterative schemes for *ab initio* total-energy calculations using a plane-wave basis set, *Phys. Rev. B* **54**, 11169 (1996).
- [34] J. P. Perdew, K. Burke, and M. Ernzerhof, Generalized Gradient Approximation Made Simple, *Phys. Rev. Lett.* **77**, 3865 (1996).
- [35] A. I. Liechtenstein, V. I. Anisimov, and J. Zaanen, Density-functional theory and strong interactions: Orbital ordering in Mott-Hubbard insulators, *Phys. Rev. B* **52**, R5467 (1995).
- [36] M. M. Markina, B. V. Mill, E. A. Zvereva, A. V. Ushakov, S. V. Streltsov, and A. N. Vasiliev, Magnetic phase diagram and first-principles study of $\text{Pb}_3\text{TeCo}_3\text{V}_2\text{O}_{14}$, *Phys. Rev. B* **89**, 104409 (2014).
- [37] Yu. V. Knyazev, N. B. Ivanova, O. A. Bayukov, N. V. Kazak, L. N. Bezmaternykh, and A. D. Vasiliev, Evolution of the Mössbauer spectra of ludwigite $\text{Co}_{3-x}\text{Fe}_x\text{O}_2\text{BO}_3$ with substitution of iron for cobalt, *Phys. Solid State* **55**, 1175 (2013).
- [38] Yu. V. Knyazev, N. V. Kazak, I. I. Nazarenko, S. N. Sofronova, N. D. Rostovtsev, J. Bartolomé, A. Arauzo, and S. G. Ovchinnikov, Effect of magnetic frustrations on magnetism of the Fe_3BO_5 and Co_3BO_5 ludwigites, *J. Magn. Magn. Mater.* **474**, 493 (2019).

- [39] G. Thornton, I. W. Owen, and G. P. Diakun, The two-band model of the LaCoO₃ semiconductor-metal transition: a spectroscopic evaluation, *J. Phys.: Condens. Matter* **3**, 417 (1991).
- [40] O. Haas, R. P. W. J. Struis, and J. M. McBreen, Synchrotron x-ray absorption of LaCoO₃ perovskite, *J. Solid State Chem.* **177**, 1000 (2004).
- [41] V. A. Dudnikov, N. V. Kazak, Yu.S. Orlov, S. N. Vereshchagin, S.Yu. Gavrilkin, A.Yu. Tsvetkov, M. V. Gorev, A. A. Veligzhanin, A. L. Trigub, I. O. Troyanchuk, and S. G. Ovchinnikov, Structural, magnetic, and thermodynamic properties of ordered and disordered cobaltite Gd_{0.1}Sr_{0.9}CoO_{3-δ}, *J. Exp. Theor. Phys.* **128**, 630 (2019).
- [42] B. Henne, V. Ney, K. Ollefs, F. Wilhelm, A. Rogalev, and A. Ney, Magnetic interactions in the Zn-Co-O system: Tuning local structure, valence and carrier type from extremely Co doped ZnO to ZnCo₂O₄, *Sci. Rep.* **5**, 16863 (2015).
- [43] M. Platonov, N. Kazak, V. Dudnikov, V. Temerov, I. Gudim, Y. Knyazev, S. Gavrilkin, V. Dyadkin, I. Dovgaliuk, D. Chernyshov, A. Hen, F. Wilhelm, A. Rogalev, and S. Ovchinnikov, Element selective magnetism in Ho_{0.5}Nd_{0.5}Fe₃(BO₃)₄ single crystal probed with hard x-ray magnetic circular dichroism, *J. Magn. Magn. Mater.* **479**, 312 (2019).
- [44] O. Mathon, F. Baudelet, J.-P. Itié, S. Pasternak, A. Polian, and S. Pascarelli, XMCD under pressure at the Fe K edge on the energy-dispersive beamline of the ESRF, *J. Synchrotron Rad.* **11**, 423 (2004).
- [45] M. S. Platonov, S. G. Ovchinnikov, N. V. Kazak, N. B. Ivanova, V. N. Zabluda, E. Weschke, E. Schierle, and K. V. Lamonova, Identification of local magnetic contributions in a Co₂FeBO₅ single crystal by XMCD spectroscopy, *JETP Lett.* **96**, 650 (2013).
- [46] R. L. Carlin, *Magnetochemistry* (Springer Science & Business Media, Springer-Verlag, Berlin, Heidelberg, 2012).
- [47] T. Kawano, H. Morito, and H. Yamane, Synthesis and characterization of manganese and cobalt pyroborates: M₂B₂O₅ (M = Mn, Co), *Solid State Sci.* **12**, 1419 (2010).
- [48] N. V. Kazak, M. S. Platonov, N. B. Ivanova, Yu.V. Knyazev, L. N. Bezmaternykh, E. V. Eremin, A. D. Vasil'ev, O. A. Bayukov, S. G. Ovchinnikov, D. A. Velikanov, and Ya.V. Zubavichus, Crystal structure and magnetization of a Co₃B₂O₆ single crystal, *J. Exp. Theor. Phys.* **117**, 94 (2013).
- [49] H. Hagiwara, H. Sato, M. Iwaki, Y. Narumi, and K. Kindo, Quantum magnetism of perfect spin tetrahedra in Co₄B₆O₁₃, *Phys. Rev. B* **80**, 014424 (2009).
- [50] N. V. Kazak, M. S. Platonov, Yu.V. Knyazev, E. M. Moshkina, S.Yu. Gavrilkin, O. A. Bayukov, M. V. Gorev, E. I. Pogoreltsev, G. M. Zeer, S. M. Zharkov, and S. G. Ovchinnikov, Fe-induced enhancement of antiferromagnetic spin correlations in Mn_{2-x}Fe_xBO₄, *J. Magn. Magn. Mater.* **452**, 90 (2018).
- [51] E. M. Carnicom, K. Górnicka, T. Klimczuk, and R. J. Cava, The homometallic warwickite V₂OBO₃, *J. Solid State Chem.* **265**, 319 (2018).
- [52] D. G. Onn, H. Meyer, and J. P. Remeika, Calorimetric study of several rare-earth gallium garnets, *Phys. Rev.* **156**, 663 (1967).
- [53] D. Piowarska, P. Gnutek, and Cz. Rudowicz, Origin of the ground Kramers doublets for Co²⁺ (3d⁷) ions with the effective spin 3/2 versus the fictitious 'spin' 1/2, *Appl. Magn. Reson.* **50**, 797 (2019).
- [54] A. Abragam and B. Bleaney, *Electron Paramagnetic Resonance of Transition Ions* (Clarendon Press Oxford, Oxford, 1970).
- [55] Z. Hao, C. Wendan, and H. Zixiang, Synthesis and crystal structure of borate oxide Co₃BO₅, *Chin. J. Struct. Chem.* **2**, 97 (2001).
- [56] See Supplemental Material at <http://link.aps.org/supplemental/10.1103/PhysRevB.103.094445> for details of the crystal structure.
- [57] G. M. Cai, L. Wang, L. M. Su, H. S. Liu, and Z. P. Jin, Sub-solidus phase relations in CoO-In₂O₃-B₂O₃ system and crystal structure of Co_{3-x}In_xBO₅ solid solution for 0 < x ≤ 1, *J. All. Com.* **615**, 809 (2014).
- [58] M. H. Cohen and F. Reif, Quadrupole effects in nuclear magnetic resonance studies of solids, *Solid State Phys.* **5**, 321 (1957).
- [59] R. M. Wood and G. J. Palenik, Bond valence sums in coordination chemistry. A simple method for calculating the oxidation state of cobalt in complexes containing only Co-O bonds, *Inorg. Chem.* **37**, 4149 (1998).
- [60] Yu.S. Orlov, L. A. Solovyov, V. A. Dudnikov, A. S. Fedorov, A. A. Kuzubov, N. V. Kazak, V. N. Voronov, S. N. Vereshchagin, N. N. Shishkina, N. S. Perov, K. V. Lamonova, R.Yu. Babkin, Yu.G. Pashkevich, A. G. Anshits, and S. G. Ovchinnikov, Structural properties and high-temperature spin and electronic transitions in GdCoO₃: experiment and theory, *Phys. Rev. B* **88**, 235105 (2013).
- [61] M. Tachibana, T. Yoshida, H. Kawaji, T. Atake, and E. Takayama-Muromachi, Evolution of electronic states in RCoO₃ (R = rare earth): heat capacity measurements, *Phys. Rev. B* **77**, 094402 (2008).
- [62] K. Knizek, Z. Jirak, J. Hejtmanek, M. Veverka, M. Marysko, G. Maris, and T. T. M. Palstra, Structural anomalies associated with the electronic and spin transitions in LnCoO₃, *Eur. Phys. J. B* **47**, 213 (2005).
- [63] B. Raveau and Md. M. Seikh, *Cobalt Oxides. From Crystal Chemistry to Physics* (Wiley-VCH, Weinheim, Germany, 2012).
- [64] N. B. Ivanova, S. G. Ovchinnikov, M. M. Korshunov, and N. V. Kazak, Specific features of spin, charge, and orbital ordering in cobaltites, *Phys. Usp.* **52**, 789 (2009).
- [65] Yu. S. Orlov, V. A. Dudnikov, M. V. Gorev, S. N. Vereshchagin, L. A. Solov'ev, and S. G. Ovchinnikov, Thermal properties of rare earth cobalt oxides and of La_{1-x}Gd_xCoO₃ solid solutions, *JETP Lett.* **103**, 607 (2016).
- [66] R. D. Shannon, Revised effective ionic radii and systematic studies of interatomic distances in halides and chalcogenides, *Acta Crystallogr. Sect. A* **32**, 751 (1976).
- [67] N. V. Kazak, M. S. Platonov, Yu.V. Knyazev, E. M. Moshkina, L. A. Solovyov, S. N. Vereshchagin, Yu.L. Mikhlin, A. A. Veligzhanin, A. L. Trigub, and S. G. Ovchinnikov, Study of mixed-valence Mn₂BO₄ using XRD, XPS and XAFS spectroscopies, *Physica B* **560**, 228 (2019).
- [68] J. Schaefer and K. Bluhm, Zur Kristallstruktur von Cu₂M(BO₃)O₂ (M = Fe³⁺, Ga³⁺), *Z. Anorg. Allg. Chem.* **621**, 571 (1995).
- [69] G. A. Petrakovskii, L. N. Bezmaternykh, D. A. Velikanov, A. M. Vorotynov, O. A. Bayukov, and M. Schneider, Magnetic properties of single crystals of ludwigites Cu₂MBO₅ (M = Fe³⁺, Ga³⁺), *Phys. Solid State*, **51**, 2077 (2009).

- [70] K. N. Boldyrev, M. N. Popova, M. Bettinelli, V. L. Temerov, I. A. Gudim, L. N. Bezmaternykh, and N. I. Leonyuk, Quality of the rare earth aluminum borate crystals for laser applications, probed by high-resolution spectroscopy of the Yb^{3+} ion, *Opt. Mater.* **34**, 1885 (2012).
- [71] N. V. Kazak, N. B. Ivanova, V. V. Rudenko, S. G. Ovchinnikov, A. D. Vasil'ev, and Yu.V. Knyazev, Conductivity study of $\text{Co}_3\text{O}_2\text{BO}_3$ and $\text{Co}_{3-x}\text{Fe}_x\text{O}_2\text{BO}_3$ oxyborates, *Solid State Phenom.* **152–153**, 104 (2009).